1962

Elastic properties of magnesium silicide

William Barclay Whitten
Iowa State University

ELASTIC PROPERTIES OF MAGNESIUM SILICIDE

by

William Barclay Whitten

A Dissertation Submitted to the
Graduate Faculty in Partial Fulfillment of
The Requirements for the Degree of
DOCTOR OF PHILOSOPHY

Major Subject: Physics

Approved:

Signature was redacted for privacy.

In Charge of Major Work

Signature was redacted for privacy.

Head of Major Department

Signature was redacted for privacy.

Dean of Graduate College

Iowa State University
Of Science and Technology
Ames, Iowa

1962

TABLE OF CONTENTS

		Page
	ABSTRACT	vi
I.	INTRODUCTION	1
II.	MEASUREMENT OF THE SOUND VELOCITIES	4
	A. Description of the Apparatus	4
	B. Construction of the Composite Oscillator	8
III.	EXPERIMENTAL RESULTS	11
	A. Analysis of Data	11
	B. Sound Velocities	13
IV.	CALCULATIONS	18
	A. The Adiabatic Elastic Constants	18
	B. Lattice Vibrations	19b
	1. Point charge model	19b
	2. The shell model	28
	3. Evaluation of constants	32
	4. Frequency spectrum	34
	C. Specific Heat	40
	D. Bonding and Ionicity	49
V.	SUMMARY	53
VI.	LITERATURE CITED	55
VII.	ACKNOWLEDGMENTS	58
VIII.	APPENDIX A: SOUND VELOCITY DATA	59
IX.	APPENDIX B: ADIABATIC ELASTIC CONSTANTS	62
X.	APPENDIX C: COULOMB COUPLING COEFFICIENTS	63

			Page
XI.	APPENDIX D:	NONCOULOMB COUPLING COEFFICIENTS	67
XII.	APPENDIX E:	EVALUATION OF THE ELASTIC CONSTANTS	70
XIII.	APPENDIX F:	HIGH AND LOW FREQUENCY DIELECTRIC CONSTANTS	72

LIST OF TABLES

		Page
Table 1.	Temperature range of transducer coupling materials	9
Table 2.	Elastic constants and their derivatives at 300 ^{o}K	19b
Table 3.	Calculated specific heat and Debye temperature	43
Table 4.	Experimental values for C_p, C_v, and θ_D, for different values of the Nernst-Lindemann constant	47
Table 5.	Room temperature elastic constants of various materials	52
Table 6.	Sound velocity, [110] direction, longitudinal wave	59
Table 7.	Sound velocity, [110] direction, shear wave I	60
Table 8.	Sound velocity, [110] direction, shear wave II	60
Table 9.	Sound velocity, [111] direction, longitudinal wave	61
Table 10.	Sound velocity, [111] direction, shear wave	61
Table 11.	Adiabatic elastic constants	62
Table 12.	[100] parameters for coulomb coupling coefficients	64
Table 13.	[111] parameters for coulomb coupling coefficients	65
Table 14.	[110] parameters for coulomb coupling coefficients	66
Table 15.	Nearest neighbors and their relative positions	69

LIST OF FIGURES

		Page
Figure 1.	Sample holder	5
Figure 2.	n versus frequency, V_{SI110}, 300 ^{o}K	14
Figure 3.	Sound velocities along [110] direction	15
Figure 4.	Sound velocities along [111] direction	16
Figure 5.	Elastic constants versus temperature	20
Figure 6.	Lattice frequencies versus q, [100] direction	36
Figure 7.	Lattice frequencies versus q, [111] direction	37
Figure 8.	Lattice frequencies versus q, [110] direction	38
Figure 9.	Lattice frequencies versus q, [100] direction	39
Figure 10.	Lattice vibration frequency distribution	41
Figure 11.	Specific heat of magnesium silicide	44
Figure 12.	Debye temperature versus temperature	46

ABSTRACT

The adiabatic elastic constants of magnesium silicide have been determined from 80 to 300 ^{o}K. The longitudinal and transverse sound velocities were measured in the [110] and [111] crystallographic directions by a resonance technique. Values for the three elastic constants at 300 ^{o}K are: C_{11} = (12.06 ± 0.17) x 10^{11} d/cm^2, C_{12} = (2.22 ± 0.18) x 10^{11} d/cm^2, C_{44} = (4.64 ± 0.05) x 10^{11} d/cm^2.

The frequencies of the lattice vibrations have been calculated along the three principal symmetry directions from the elastic constants and the reststrahl frequency, and an approximate frequency distribution was obtained. The lattice specific heat was calculated at several temperatures from this distribution. From the elastic constants, a value of 578 ^{o}K was obtained for the Debye temperature at absolute zero. The Debye approximation is not valid above 10 ^{o}K.

I. INTRODUCTION

The semiconducting properties of magnesium silicide have been studied by several investigators, particularly by Heller and Danielson (1), Morris et al. (2), Winkler (3), and Koenig et al. (4). The interpretation of their experimental results by existing semiconductor theories has been hindered because certain mechanical and thermal properties of this material are not known. Some of these properties can be calculated fairly accurately from the elastic constants. Macroscopic properties such as the compressibility and Debye temperature can be obtained directly. From a microscopic point of view, the elastic constants can give some information about the binding mechanisms in the material. They are also useful in the evaluation of force constants for lattice vibration and specific heat calculations. It is hoped that the present investigation will furnish a useful description of the elastic properties of magnesium silicide and the general features of the phonon frequency distribution.

The elastic stiffness constants relate the six independent stress and strain components in a material. For a cubic crystal, there are only three independent elastic constants, C_{11}, C_{12}, and C_{44}. The elastic constants can be determined by measuring the strains resulting from

appropriately applied static stresses, or by measuring the velocities of sound waves in various directions in the crystal. The latter method was chosen for the present investigation. DeLaunay (5) has given, in terms of the density ρ, the following expressions for the sound velocities along the principal symmetry directions for a cubic crystal.

In the [100] direction, for a longitudinal wave,

$$v_L^2 = C_{11}/\rho \ ; \qquad \text{(Eq. 1)}$$

and, for a shear wave,

$$v_S^2 = C_{44}/\rho \ . \qquad \text{(Eq. 2)}$$

In the [111] direction, for a longitudinal wave,

$$v_L^2 = (C_{11} + 2C_{12} + 4C_{44})/3\rho \ ; \qquad \text{(Eq. 3)}$$

and, for a shear wave,

$$v_S^2 = (C_{11} - C_{12} + C_{44})/3\rho \ . \qquad \text{(Eq. 4)}$$

In the [110] direction, for a longitudinal wave,

$$v_L^2 = (C_{11} + C_{12} + 2C_{44})/2\rho \ . \qquad \text{(Eq. 5)}$$

For a shear wave polarized along [100] direction,

$$v_{SI}^2 = C_{44}/\rho \ ; \qquad \text{(Eq. 6)}$$

and, for a shear wave polarized along [$\bar{1}$10] direction,

$$v_{SII}^2 = (C_{11} - C_{12})/2\rho \ . \qquad \text{(Eq. 7)}$$

At least three of these velocities must be measured to determine the three elastic constants. A detailed treatment of the elastic properties of solids and the ways in which they are determined can be found in a recent review article by Huntington (6).

II. MEASUREMENT OF THE SOUND VELOCITIES

A. Description of the Apparatus

A resonance technique was chosen for sound velocity measurements in magnesium silicide. Large crystals of good quality could not be obtained so the measurements had to be made on small specimens with high attenuation coefficients. The pulse-echo technique which is well known for its convenience and accuracy is not suited for crystals of this type since the precision of the measurements decreases rapidly when only a few closely-spaced echoes can be observed.

Specimens with two parallel faces perpendicular to the desired crystallographic axes were sandwiched between two quartz transducers in the sample holder shown in Figure 1. The transducers had a resonant frequency of ten megacycles and were either X-cut or Y-cut, so that either longitudinal or shear velocities could be measured. The outer face of each transducer was coated with a thin film of conducting paint and a wire was soldered to the side of the specimen for a common lead.

One transducer was excited with the 1,000 cycle modulated output (~ 1 v rms.) of a General Radio model 805C signal generator which was swept in frequency from about five to fifteen megacycles. Sound waves produced in the

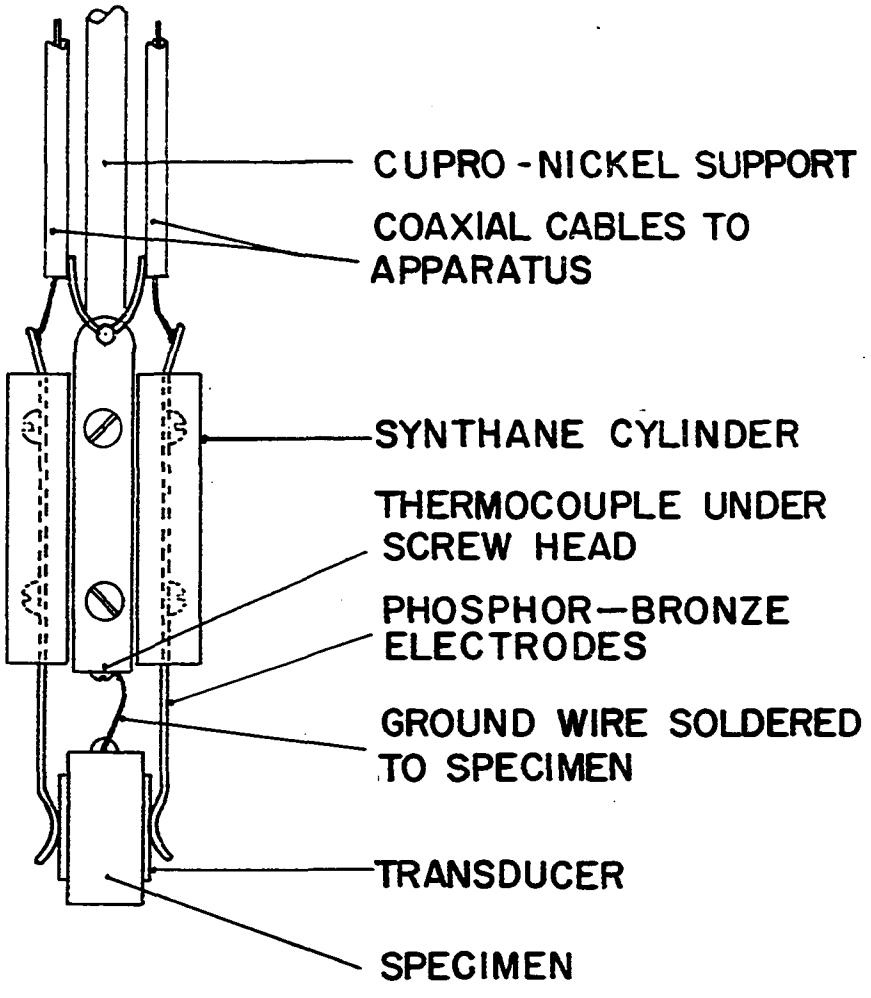

Figure 1. Sample holder

specimen by this transducer generated a signal across the second transducer. This signal was amplified by a Hewlett-Packard model 460A wide-band amplifier and demodulated with a microwave silicon diode. The resulting 1,000 cycle signal was amplified by a high gain audio amplifier, rectified, and displayed on a sensitive microammeter.

At the resonant frequencies of the system composed of the specimen, transducers, and coupling films, a marked increase in the signal from the second transducer was observed. The frequencies of these resonances were measured with a Berkeley model 5571 counter or a Signal Corps BC221 frequency meter. The frequencies were recorded to the nearest kilocycle, which corresponded roughly to the reproducibility of the signal generator setting at the lower frequencies. At frequencies above ten megacycles the reproducibility was not as good due to the logarithmic character of the generator dial.

Fine structure on the resonances was occasionally observed when the bonds were very rigid. Similar effects have been seen by other investigators (7, 8). In such cases, the frequency of the largest peak was recorded. The resonances were observed to be alternately expanded and contracted in frequency, but the frequency interval between every other resonance was roughly constant. The amount of these deviations was smallest near the resonant frequency of the

transducer and could be varied somewhat by changing the transducer bonds. The deviation was also observed to be more pronounced in crystals with a high attenuation. In some measurements on the sodium tungsten bronzes, the resonances for some specimens were broadened in such a way that every other pair of resonances appeared as a single broad hump in the output voltage versus frequency curve. This phenomenon probably can be ascribed to the losses in the specimen and bonds. It is believed that the velocities calculated from the average frequency increment are not affected by these deviations except that the scatter in the data reduces the accuracy of the transducer and bond correction described later.

A copper-constantan thermocouple was used to measure and control the temperature at which a measurement was being made. The thermocouple was checked at the boiling point of liquid oxygen and a correction to the standard Leeds and Northrop thermocouple table was obtained. The thermocouple voltages were measured on a Rubicon type B potentiometer with a Leeds and Northrop type E galvanometer.

Two cadmium sulfide photocells mounted on the galvanometer were used to control the temperature. The photocells activated relays which switched the heater current and were arranged so that a damping action was introduced whenever the temperature oscillations exceeded approximately $0.1^{\circ}K$,

enabling the temperature to be controlled to within 0.5°K during a measurement.

B. Construction of the Composite Oscillator

The specimens were cut from irregularly-shaped crystals of magnesium silicide grown by co-workers Marvin W. Heller and William L. Smith. One piece was oriented for sound propagation along the [110] crystallographic direction, another for propagation in the [111] direction. The crystal axes were located by Laue back-reflection x-ray photographs using copper or molybdenum targets.

Two parallel faces normal to the direction of sound propagation were generated by hand lapping on emery paper. The alignment error was about 2° for the [110] specimen, and less than 1° for the [111] specimen. The [110] sample was about 1.5 cm in diameter and 0.8 cm thick. The [111] sample was roughly 1.2 cm in diameter and 0.6 cm thick. The sides of the samples were not machined except for the removal of some irregular corners.

Several different bonding materials were required for satisfactory transducer coupling over the temperature range. The materials used and their useful temperature ranges are shown in Table 1. At the low temperature limits indicated, the bonds would fracture due to the differential expansion of the transducer and specimen. Accurate measurements could

Table 1. Temperature range of transducer coupling materials

Material	Mode	T_{min}	T_{max}
Phenyl salicylate	Longitudinal	240°K	>300°K
	Transverse	240°K	>300°K
Glycerin	Longitudinal	100°K	230°K
	Transverse	100°K	230°K
Silicone grease[a]	Longitudinal	<80°K	240°K
	Transverse	<80°K	170°K

[a]Dow Corning Silicone Stopcock Grease.

not be made above the high temperature limits because of softening of the bonds.

In most cases, a small quantity of 3200 mesh emery was added to the coupling material to ensure a fairly uniform and reproducible bond. For the corrections described later for the transducers and bonds, it was desirable for the transducers to be parallel to the faces of the specimen, and for the two bonds to be of approximately the same thickness.

Bolef and Menes (7) have described a somewhat similar technique for measuring sound velocities. They use only one transducer and detect the resonances with a Q meter. The correction for the transducer and bond is still required but

would be only half as large. This is certainly a benefit and if the method works well for materials with high acoustic attenuation, its accuracy should be as good as or better than that of the technique used for the present investigation.

III. EXPERIMENTAL RESULTS

A. Analysis of Data

Accurate calculation of the sound velocities from the resonant frequencies of the composite oscillator described in the previous section requires a knowledge of the corrections which must be considered for the transducers and bonds. Williams and Lamb (9) have calculated by transmission line theory the phase shift undergone by a sound wave upon reflection from a surface to which a transducer is coupled by a third material. If Z_T, Z_S, and Z_F are the acoustic impedances, ρv, of the transducer, specimen, and coupling film, respectively, the phase shift is given by

$$\varphi = \pi - 2\tan^{-1}\left[\frac{Z_F}{Z_S}\,\frac{Z_T\tan\theta_T + Z_F\tan\theta_F}{Z_F - Z_T\tan\theta_T\tan\theta_F}\right], \qquad \text{(Eq. 8)}$$

where $\theta_T = \pi f/f_T$,

$\theta_F = \pi f/f_F$,

f_T and f_F being the resonant frequencies of the transducer and film, and f being the frequency of the sound wave. The resonance condition for the system composed of a parallel-faced specimen with transducers coupled to opposite faces is that a sound wave twice reflected be in phase at a given

point in the specimen with a wave reflected 2m times, or

$$\frac{2\pi\ell f}{v} - \varphi = n\pi, \quad n = 0, 1, 2.....$$

where ℓ is the length of the sample and v is the sound velocity.

For the analysis of the experimental data, Equation 8 was simplified with the approximation that Z_F is small compared to Z_T, and f_F is much larger than the frequencies of the measurements. In this approximation, the resonance condition can be reduced to

$$n = \frac{2\pi\ell f}{v} + \frac{2}{\pi} \tan^{-1} \left[\frac{Z_T}{Z_S} \frac{\tan \theta_T}{1 - (\pi Z_T / f_F Z_F) f \tan \theta_T}\right]. \qquad \text{(Eq. 9)}$$

The velocity calculated from Equation 9 is quite insensitive to errors in Z_S so a value for Z_S can be obtained from the density of the specimen and the uncorrected sound velocity.

The velocities were calculated on an IBM 704 computer. The squared deviations of the quantities

$$n - \frac{2}{\pi} \tan^{-1} \left[\frac{Z_T}{Z_S} \frac{\tan \theta_T}{1 - (\pi Z_T / f_F Z_F) f \tan \theta_T}\right]$$

from the straight line,

$$n' = \frac{2\pi\ell f}{v} + n_o \qquad \text{(Eq. 10)}$$

were minimized by adjusting the quantity $\pi Z_T/f_F Z_F$. In Equation 10, n' is now no longer an integer, and n_o is an arbitrary constant. The velocity can be readily obtained from the slope of Equation 10. In Figure 2, one of the better sets of experimental points is shown along with the line obtained by the computer. This comparison shows clearly the deviations encountered when the denominator of the argument of the arctangent in Equation 9 goes through zero.

Some systematic deviations in the calculated velocities were found when different bonds were employed at the same temperature. These deviations were primarily caused by scatter in the data resulting from the alternate contractions of the resonances in the frequency range where the phase shift is changing rapidly. This effect was most pronounced for measurements of the higher velocities, where fewer resonances were observed.

B. Sound Velocities

The three velocities in the [110] direction and two velocities in the [111] direction are shown as functions of temperature in Figures 3 and 4. Where more than one value was obtained at a given temperature, the average is shown. Sample lengths were measured at room temperature with a

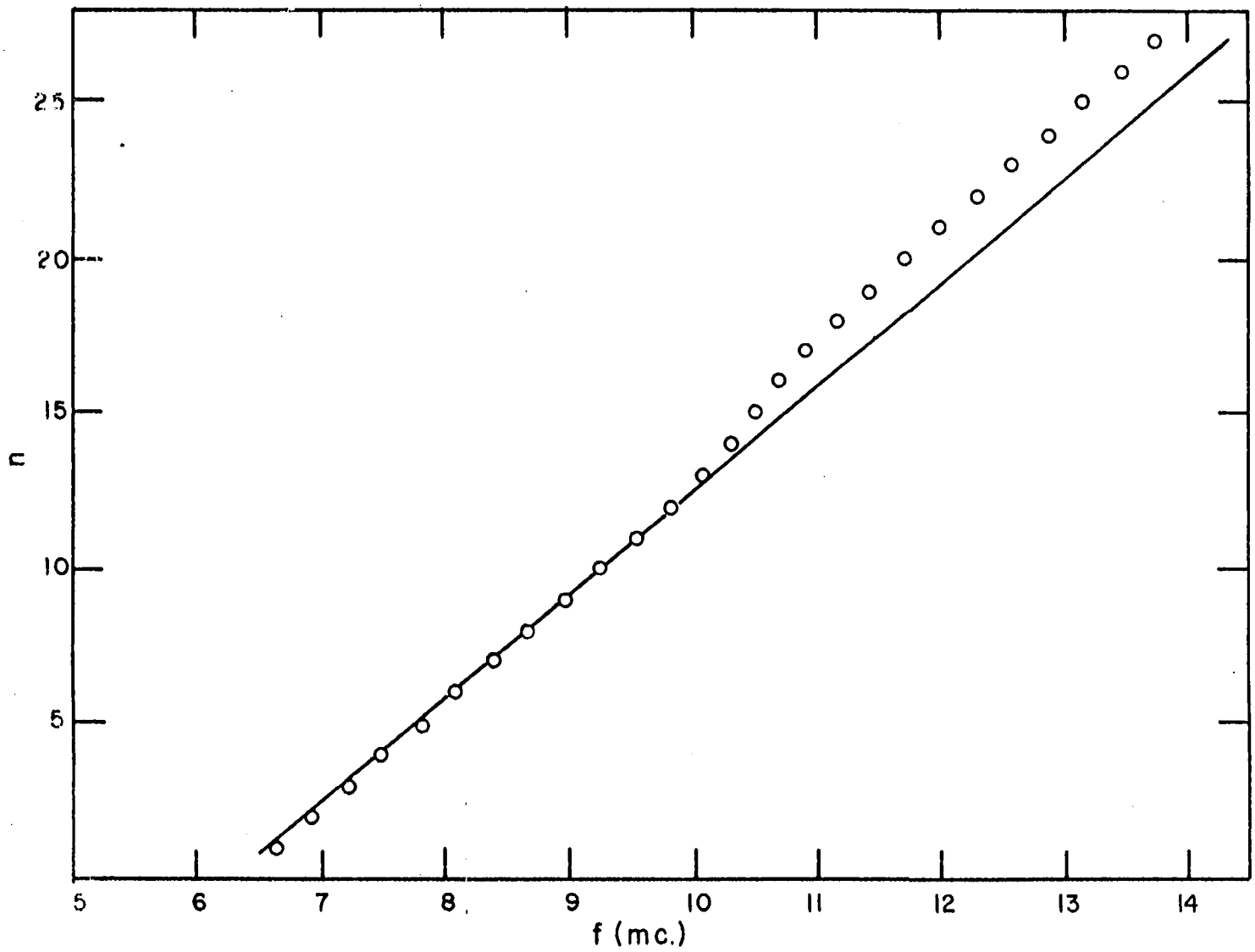

Figure 2. n versus frequency, V_{SI110}, 300 ^{o}K

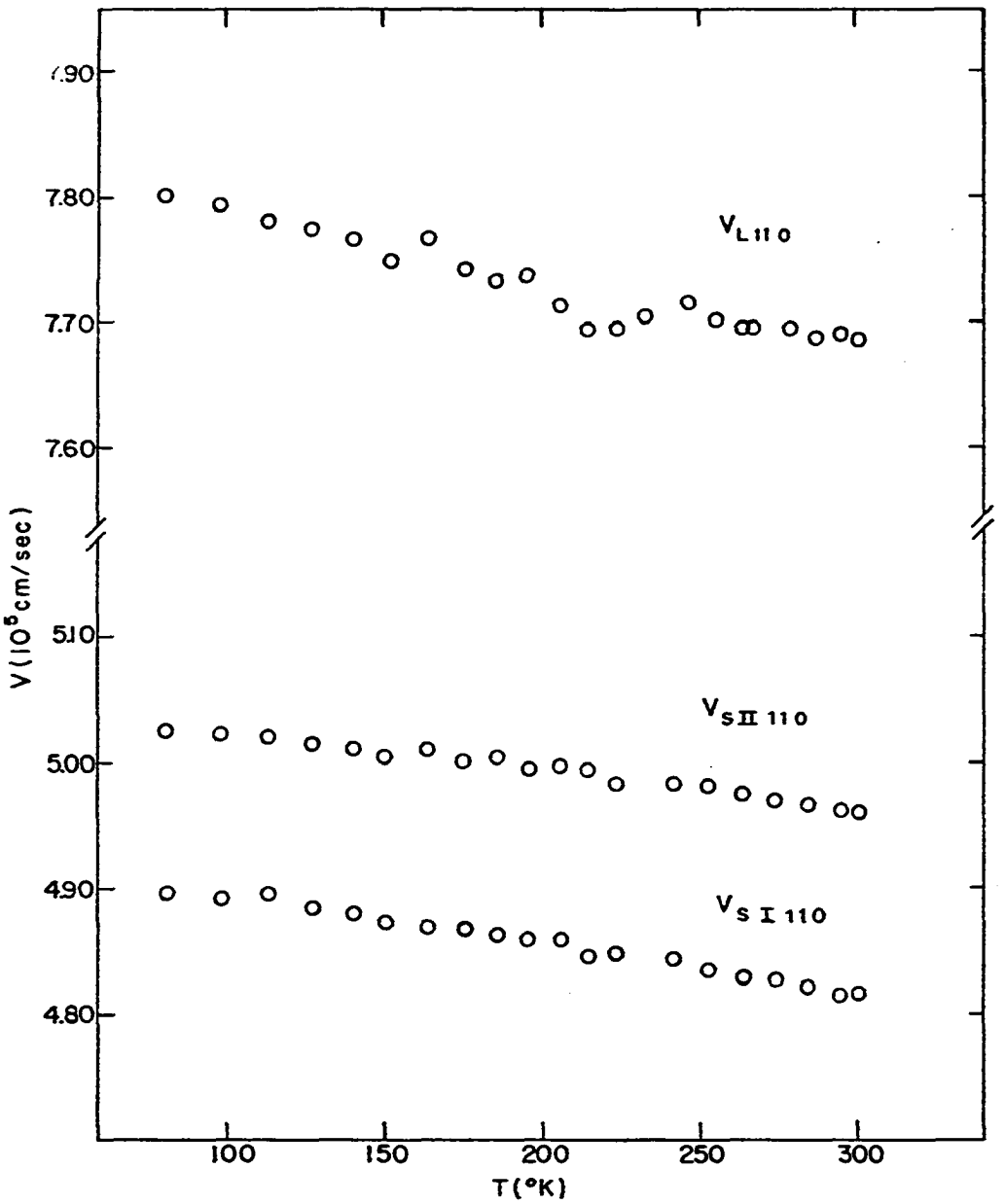

Figure 3. Sound velocities along [110] direction

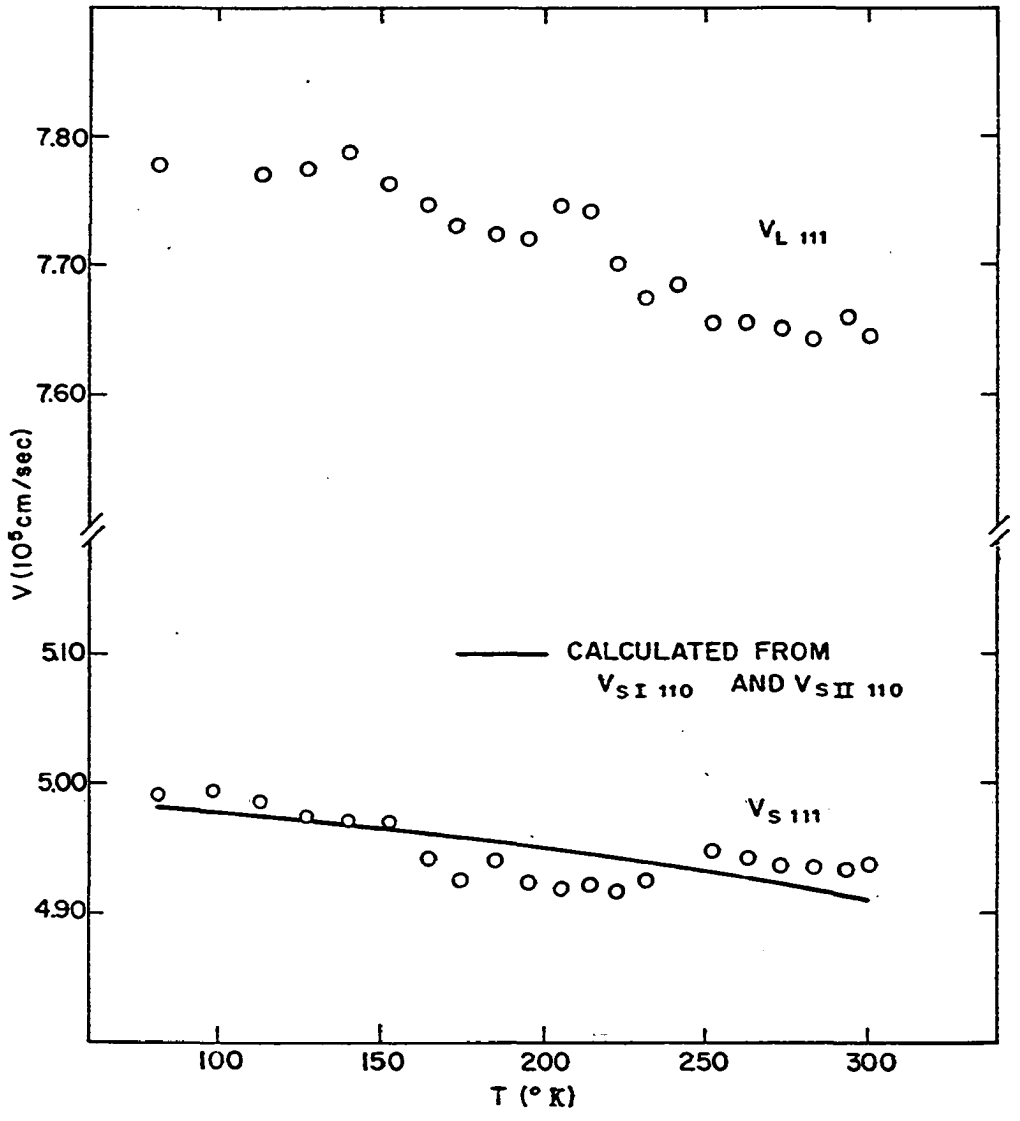

Figure 4. Sound velocities along [111] direction

micrometer and the linear expansion data of Born[1] were used to determine the lengths at other temperatures.

The principal source of error was the correction for the transducers and bonds. As mentioned in the preceding section, some systematic deviations in the velocities were noted when different bonds were used. No noticeable deviations were found for the [110] shear velocities, but variations of up to 1% were observed in the other three velocities at various temperatures.

The random fluctuations with temperature of the velocities shown in Figures 3 and 4 are a fair indication of the precision of the measurements. On the basis of these fluctuations and the systematic errors due to the transducer and bond correction, the [110] shear measurements are estimated to be accurate to 0.5%, the remainder to 1%. These errors are larger than most of the values reported in the recent literature for measurements on other materials, but it is felt that the results are sufficiently accurate for most calculations, at least until better crystals can be obtained.

---

[1]Born, Harold. Illinois State Normal University. Normal, Illinois. Linear thermal expansion of magnesium silicide. Private communication. 1959.

IV. CALCULATIONS

A. The Adiabatic Elastic Constants

While the elastic properties of a material could be discussed in terms of the sound velocities in a material and the density, the velocities are not all independent so there would be some redundancy. It is much more convenient to use the elastic stiffness constants, or elastic constants, of which there are only three for a cubic material. The elastic constants directly relate the components of stress and strain--a function useful to the physicist as well as the engineer. The theorist often works with the relative displacements of atoms, or strains, while the experimentalist is more interested in stresses, which are easier to measure. A knowledge of the elastic constants is necessary to connect the theory with experiment.

From the five velocities which were measured, the three elastic constants were calculated twice, with combinations of the two [110] shear velocities and one of the two longitudinal velocities. The combination of the [110] shear velocities and the [111] shear velocity does not determine the three elastic constants completely, but gives an internal check of the data. Combinations of one [110] shear velocity with two [111] velocities were not used since the [111] velocities were considered less reliable than the [110] shear

velocities. The elastic constants shown in Figure 5 are averages of the values calculated in the two ways. These results are tabulated in Appendix B.

The errors are largely due to errors in the velocity measurements. One might expect, in addition, some contributions due to residual strains in the two specimens, slight differences in stoichiometry, and errors in the alignment of the propagation direction with the desired crystallographic axis. The x-ray density, 2.00 g/cm^3, corrected for thermal expansion was used for all determinations. When errors of 0.5% in the [110] shear velocities and 1% in the rest are assumed, the following contributions are obtained at room temperature: for C_{11}, 1.4%, for C_{12}, 8.1%, for C_{44}, 1.0%. The relative error for C_{12} is large because C_{12} is so small. The actual uncertainties in C_{11} and C_{12} are of comparable size. The relative errors obtained above are larger in most cases than the discrepancies between the values for the elastic constants calculated in the two ways, so they probably can be considered reasonable estimates of the total error.

Straight line fits to the elastic constants were made from 150 to 300 ^{o}K by the method of least squares. The values obtained for the elastic constants and their temperature derivatives at 300 ^{o}K are given in Table 2. Values for the adiabatic bulk modulus, B, given by

$$B = (C_{11} + 2C_{12})/3$$

and its temperature derivative are also given. The uncertainties in the elastic constants and bulk modulus are those found if we assume errors of 1.4% in C_{11}, 8.1% in C_{12}, and 1.0% in C_{44}. Some of the calculations in the following sections were made with preliminary values of the elastic constants which were slightly different, but the use of the better values would not change the results significantly.

Table 2. Elastic constants and their derivatives at 300 °K

Modulus	Value at 300 °K (10^{11} d/cm^2)	Derivative (10^8 d/cm^2 °K)
C_{11}	12.06 ± .17	-1.688
C_{12}	2.22 ± .18	-0.631
C_{44}	4.64 ± .05	-0.626
B	5.50 ± .18	-0.983

B. Lattice Vibrations

1. Point charge model

The electrical, thermal, and optical properties of solids are influenced to a large degree by the vibrations

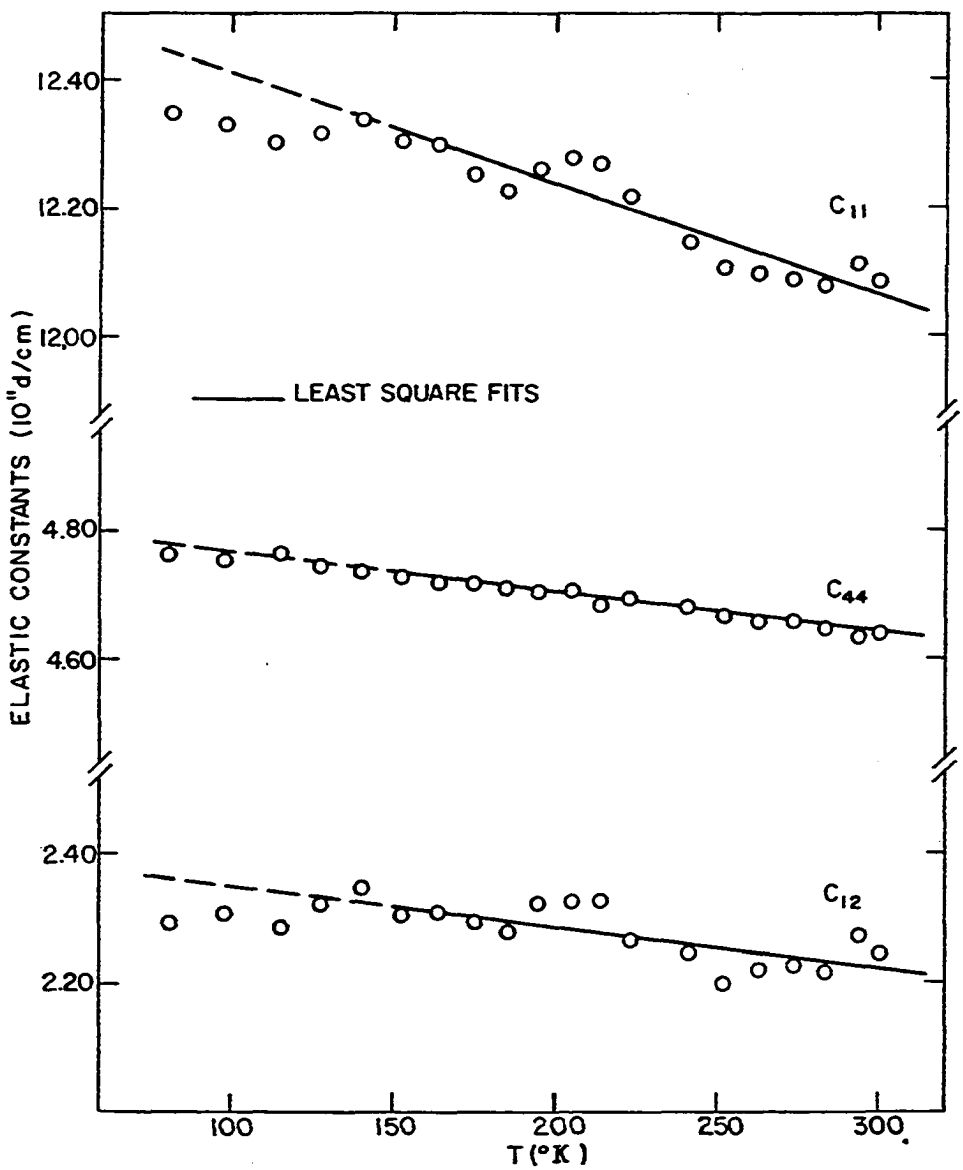

Figure 5. Elastic constants versus temperature

about their equilibrium positions of the atoms composing the solid. A detailed knowledge of these vibrations is essential for an accurate description of these properties. Fortunately, a fairly simple model originally proposed by Born and von Karman (10) and refined by many others (11, 12, 13, 14, 15) has enabled the calculation of the principal features of the lattice vibration spectra of many different materials in a straightforward, if tedious, way. Details of this model and the many refinements can be found in review articles by DeLaunay (5) and Blackman (10), and in the book by Born and Huang (12).

The frequencies of the lattice vibrations in magnesium silicide were calculated at several points in reciprocal space by a method similar to that used by Ganesan and Srinivasan (16) for calcium fluoride. The magnesium and silicon atoms were treated as point charges with appropriate masses. Central and noncentral restoring forces between nearest neighbors were assumed in addition to the long range coulomb forces.

The magnesium silicide structure is similar to that of calcium fluoride. The lattice can be generated by the vectors (17)

$$\vec{x}_{\ell} = (\ell_1, \ell_2, \ell_3)a/2$$

where the ℓ_i are integers and $\Sigma\ell_i$ is even; a is the lattice constant. One silicon atom and two magnesium atoms, A and B, are grouped about each lattice site with relative coordinates (0, 0, 0)a/4, (-1, -1, -1)a/4, and (1, 1, 1)a/4, respectively. The three elements within a primitive cell will be designated by the index, k, k = 1, 2, 3, representing the silicon atom, magnesium atom A, and magnesium atom B. To simplify the notation somewhat, the index ℓ will be used to represent the three cell indices, ℓ_1, ℓ_2, and ℓ_3.

The equations of motion for the various elements of the crystal can be derived in the following manner, as described by Born and Huang (12). Let φ be the total potential energy of the lattice. The equilibrium position of the kth element in the ℓth cell will be denoted by $\vec{x}(\ell k)$, the displacement from the equilibrium position by $\vec{u}(\ell k)$. The equations of motion for any element of the crystal can be written

$$m_k \ddot{u}_\alpha(\ell k) = - \frac{\partial \varphi}{\partial u_\alpha(\ell k)} \qquad \alpha = 1, 2, 3 . \qquad \text{(Eq. 11)}$$

The standard treatment is to expand φ to second order in the displacements about the equilibrium positions of all the elements, giving

$$\varphi = \varphi_o + \sum_{\beta \ell k} \left(\frac{\partial \varphi}{\partial u_\beta(\ell k)}\right)_o u_\beta(\ell k)$$

$$+ \sum_{\substack{\gamma \ell \, k \\ \beta \ell' k'}} \left(\frac{\partial^2 \varphi}{\partial u_\gamma(\ell k) \partial u_\beta(\ell' k')}\right)_o u_\gamma(\ell k) u_\beta(\ell' k') \qquad \text{(Eq. 12)}$$

The constant term φ_o can be removed by a suitable choice of a reference level and the coefficients $\left(\frac{\partial \varphi}{\partial u_\beta(\ell k)}\right)_o$ vanish for a stable lattice. The equations of motion then become

$$m_k \ddot{u}_\alpha(\ell k) = - \sum_{\beta \ell' k'} \left(\frac{\partial^2 \varphi}{\partial u_\alpha(\ell k) \partial u_\beta(\ell' k')}\right)_o u_\beta(\ell' k') \; . \qquad \text{(Eq. 13)}$$

We would like a plane wave solution of the form

$$u_\alpha(\ell k) = A_\alpha^k \, e^{\, i[\vec{q} \cdot \vec{x}(\ell k) - \omega t]} \qquad \text{(Eq. 14)}$$

where $\vec{q}$ is the wave vector of magnitude 2π times the reciprocal wave length and parallel to the direction of propagation. Substitution shows that Equation 14 can be a solution if the secular determinant

$$\left| \left[{}^{kk'}_{\alpha\beta}\right] - m_k \omega^2 \delta_{\alpha\beta} \delta_{kk'} \right|$$

vanishes. The coupling coefficients, $\left[{}^{kk'}_{\alpha\beta}\right]$, are defined by

$$\left[{}^{kk'}_{\alpha\beta}\right] = \sum_{\ell'} \left(\frac{\partial^2 \varphi}{\partial u_\alpha(\ell k) \partial u_\beta(\ell' k')}\right)_o e^{\, i\vec{q} \cdot [\vec{x}(\ell' k') - \vec{x}(\ell k)]} \qquad \text{(Eq. 15)}$$

We can find the allowed frequencies for a given value of $\vec{q}$ by solving a 3nth degree equation in ω^2, n being the number of elements in a unit cell. For the model under investigation, the secular determinant will in general be of ninth degree in ω^2, although it can be factored along the principal symmetry directions.

The total potential energy, φ, and the coupling coefficients are assumed to be separable into parts containing only coulomb interactions and parts containing only non-coulomb interactions:

$$\varphi = C_{\varphi} + N_{\varphi}$$

$$\left[{}^{kk'}_{\alpha\beta}\right] = C_{\left[{}^{kk'}_{\alpha\beta}\right]} + N_{\left[{}^{kk'}_{\alpha\beta}\right]} \qquad \text{(Eq. 16)}$$

Expressions for the coulomb coupling coefficients were developed by Kellermann (13) and adapted for the fluorite structure by Srinivasan (17). The coefficients must be evaluated numerically for each value of the wave vector, with the aid of a summation technique devised by Ewald (18, p. 571) for fast convergence. Values for certain magnitudes and directions of the wave vector have been calculated previously for other structures (13, 19) and are applicable with only slight modification. The numerical values used

in the present investigation are given in Appendix C.

The noncoulomb parts of the coupling coefficients were obtained by a method similar to that of DeLaunay (5). Central and noncentral restoring forces were assumed between nearest neighbors only. The details of the calculations can be found in Appendix D. The coefficients are the same as those of Ganesan and Srinivasan (16) except for a difference in sign convention, and are given below:

$$N\left[\begin{smallmatrix}11\\ \alpha\beta\end{smallmatrix}\right] = 8\beta\ \delta_{\alpha\beta}$$

$$N\left[\begin{smallmatrix}22\\ \alpha\beta\end{smallmatrix}\right] = N\left[\begin{smallmatrix}33\\ \alpha\beta\end{smallmatrix}\right] = 4\beta\ \delta_{\alpha\beta}$$

$$N\left[\begin{smallmatrix}23\\ \alpha\beta\end{smallmatrix}\right] = 0 \qquad \text{(Eq. 17)}$$

$$N\left[\begin{smallmatrix}12\\ \alpha\alpha\end{smallmatrix}\right] = N\left[\begin{smallmatrix}13\\ \alpha\alpha\end{smallmatrix}\right]^* = -\ 4\beta(C_1C_2C_3 + i\ S_1S_2S_3)$$

$$N\left[\begin{smallmatrix}12\\ 12\end{smallmatrix}\right] = N\left[\begin{smallmatrix}13\\ 12\end{smallmatrix}\right]^* = 4\gamma(S_1S_2C_3 + i\ C_1C_2S_3)$$

where $C_\alpha = \cos q_\alpha a/4$, $S_\alpha = \sin q_\alpha a/4$, etc. The remaining coefficients may be obtained by a cyclic permutation of the indices, α, β, and by requiring the matrix to be hermitian. In the above expressions, β and γ are force constants which are linear combinations of the central and noncentral force constants, q is the wave vector and a is the lattice

parameter.

The force constants, β and γ, and the charge on the magnesium atoms can be evaluated from the elastic constants or sound velocities. Born and Huang (12) have developed an expansion technique which yields the elastic constants as functions of the coupling coefficients and their derivatives at $q = 0$. Srinivasan (17) and Rajagopal (20) have applied this method to calcium fluoride. The derivatives of the coulomb parts of the coupling coefficients at $q = 0$ were evaluated numerically by Srinivasan. From their expressions and the noncoulomb coefficients, the following expressions for the elastic constants are derived in Appendix E:

$$aC_{11} = 3.276 \cdot 8e^2/a^3 + 2\beta$$

$$aC_{12} = -5.395 \cdot 8e^2/a^3 + 4\gamma - 2\beta \qquad \text{(Eq. 18)}$$

$$aC_{44} = -1.527 \cdot 8e^2/a^3 + 2\beta - (2.519 \cdot 8e^2/a^3 - \gamma)^2\, 2/\beta$$

where e is the charge on the magnesium atom. These results, except for slight numerical differences are the same as the expressions obtained by Ganesan and Srinivasan (16), if some of their force constants are omitted. It is believed that the above results are the more accurate, since the corrections of Rajagopal (20) have removed some previous

discrepancies.

In the limit of long wave lengths, the secular determinant reduces to three determinants of rank three. They can be written

$$\begin{vmatrix} 8\beta+e_1^2C/v-m_1\omega^2 & -4\beta+e_1e_2C/v & -4\beta+e_1e_3C/v \\ -4\beta+e_1e_2C/v & 4\beta+e_2^2C/v-m_2\omega^2 & e_2e_3C/v \\ -4\beta+e_1e_3C/v & e_2e_3C/v & 4\beta+e_3^2C/v-m_3\omega^2 \end{vmatrix} = 0 \qquad \text{(Eq. 19)}$$

where e_1, e_2, e_3, m_1, m_2, m_3 are the charges and masses of the silicon atom, magnesium A, and magnesium B, $v = a^3/4$ is the volume of a primitive cell, and C takes the value $8\pi/3$ for longitudinal vibrations, $-4\pi/3$ for transverse vibrations. For this material, $m_2 = m_3$, $e_2 = e_3$, and $e_1 = 2e_2$. By subtracting the last two rows of the determinant, one root

$$\omega^2 = 4\beta/m_2 \qquad \text{(Eq. 20)}$$

is easily obtained. This root corresponds to a vibration of the two magnesium atoms in opposite directions, leaving the silicon atom stationary so the modes with this frequency have no dipole moment. The remaining quadratic equation,

obtained from the first row and sum of the second two has the following roots:

$$\omega^2 = 0 \qquad \text{(Eq. 21)}$$

$$\omega^2 = (4\beta + 2e_2^2 C/v)(m_1 + 2m_2)/m_1 m_2 \qquad \text{(Eq. 22)}$$

The latter, with $C = -4\pi/3$, corresponds to the reststrahl frequency observed in the infrared spectrum.

2. The shell model

A model in which one or more atoms in the primitive cell is treated as a core plus a massless electronic shell has been quite successful recently in predicting the lattice vibration frequencies of germanium (14) and sodium iodide (15). A calculation of the same sort was tried for magnesium silicide, with the magnesium atoms considered to be point charges and the silicon atom treated as a positively charged core and a negatively charged massless shell coupled by a central restoring force. The noncoulomb forces between nearest neighbor magnesium and silicon atoms were assumed to act only on the silicon shell. While the above model is certainly oversimplified, it requires the evaluation of at least five parameters. For a more sophisticated model including the polarizability of the magnesium atoms and

additional restoring forces, more experimental data (such as measurements of the Raman frequency and multiple phonon infrared absorption frequencies, or inelastic neutron scattering data) would be needed.

In the long wave length limit the secular determinant for this model factors into three fourth rank determinants:

$$\begin{vmatrix} \delta+e_1^2C/v-m_1\omega^2 & -\delta+e_1e_2C/v & e_1e_3C/v & e_1e_4C/v \\ -\delta+e_1e_2C/v & 8\beta+\delta+e_2^2C/v & -4\beta+e_2e_3C/v & -4\beta+e_2e_4C/v \\ e_1e_3C/v & -4\beta+e_2e_3C/v & -4\beta+e_3^2C/v-m_3\omega^2 & e_3e_4C/v \\ e_1e_4C/v & -4\beta+e_2e_4C/v & e_3e_4C/v & 4\beta+e_4^2C/v-m_4\omega^2 \end{vmatrix} = 0 \qquad \text{(Eq. 23)}$$

Here the e_i and m_i represent charges and masses for the silicon core, shell, magnesium A, and magnesium B, respectively. δ is the force constant for the silicon core-shell interaction. The charges e_3 and e_4 and masses m_3 and m_4 are equal for this material, and total charge neutrality requires that

$$\sum_{i=1}^{4} e_i = 0 \; . \qquad \text{(Eq. 24)}$$

The secular equation has three roots:

$$\omega^2 = 0 \qquad \text{(Eq. 25)}$$

$$\omega^2 = 4\beta/m_3 \qquad \text{(Eq. 26)}$$

$$\omega^2 = \frac{m_1 + 2m_3}{m_1 m_3} \left[\frac{4\beta\delta + 4\beta e_1^2 C/v + 2\delta\, e_3^2 C/v}{(8\beta + \delta)\left(1 + \frac{e_2^2 C}{v(8\beta + \delta)}\right)}\right] \qquad \text{(Eq. 27)}$$

where C is again $8\pi/3$ for longitudinal modes and $-4\pi/3$ for transverse modes, and v is the volume of the primitive cell.

The first two roots are the same as for the point charge model. The third can be put into a form used by Woods *et al.* (15),

$$\mu\omega^2 = \frac{4\beta\delta}{8\beta + \delta} + \frac{2}{v}C \frac{\left[e_3 + \frac{4\beta e_2}{8\beta + \delta}\right]^2}{\left(1 + \frac{\alpha}{v} C\right)} . \qquad \text{(Eq. 28)}$$

In this expression, $\alpha = e_2^2/(8\beta+\delta)$ is the polarizability of the silicon atom, as will be seen later, and μ is the reduced mass, $m_1 m_3/(m_1+2m_3)$.

The high and low frequency dielectric constants can be calculated from a consideration of the dipole moment per

unit volume produced by an external electric field in the x direction, as shown in Appendix F. The calculations are almost identical to those of Woods *et al.* (15) since only one optic mode at q = 0 possesses a dipole moment. The following expressions for the polarizabilities per unit volume are obtained;

at $\omega = 0$,

$$\frac{(\alpha+\alpha_I)}{v} = \frac{P}{E_o} = \frac{1}{v}\left[\frac{e_2^2}{8\beta+\delta} + \frac{2(e_3 + \frac{4\beta e_2}{8\beta+\delta})^2}{\frac{4\beta\delta}{8\beta+\delta}}\right] , \qquad \text{(Eq. 29)}$$

at $\omega = \infty$,

$$\frac{\alpha}{v} = \frac{P}{E_o} = \frac{1}{v}\frac{e_2^2}{8\beta+\delta} , \qquad \text{(Eq. 30)}$$

where E_o is the effective field, P is the polarization, v is the volume of the primitive cell. α is the electronic polarizability of the silicon atom sir only the massless silicon shell can be displaced at the high frequency limit, and α_I can be considered the ionic polarizability of the lattice.

The high frequency dielectric constant, ϵ, is related to the electronic polarizability, α, by the relation (15)

$$\frac{4\pi\alpha}{3v} = \frac{\epsilon-1}{\epsilon+2} . \qquad \text{(Eq. 31)}$$

Similarly, the low frequency dielectric constant, ϵ_o, is found from

$$\frac{4\pi(\alpha+\alpha_I)}{3v} = \frac{\epsilon_o - 1}{\epsilon_o + 2} \cdot \qquad \text{(Eq. 32)}$$

Just as for the model of Woods et al. for the alkali halides, the longitudinal and transverse frequencies of the mode possessing a dipole moment satisfy the Lyddane, Sachs, and Teller relationship (21)

$$\left(\frac{\omega_L^2}{\omega_T^2}\right)_{q=0} = \frac{\epsilon_o}{\epsilon} \cdot \qquad \text{(Eq. 33)}$$

This relationship is not satisfied for the point charge model. The longitudinal optic mode frequency is considerably higher than that for the shell model.

3. Evaluation of constants

Three parameters may be evaluated from the room temperature elastic constants, $C_{11} = 12.12 \times 10^{11}$ d/cm^2, $C_{12} = 2.20 \times 10^{11}$ d/cm^2, $C_{44} = 4.65 \times 10^{11}$ d/cm^2. Equations 18 can be solved for β, γ and e_3, giving

$$\beta = 2.26 \times 10^4 \text{ d/cm}$$
$$\gamma = 2.78 \times 10^4 \text{ d/cm}$$
$$e_3 = \pm 5.54 \times 10^{-10} \text{esu} = \pm 1.15 e_o \text{ ,}$$

where e_o is the electronic charge. For either model, e_3 is the charge on the magnesium atom.

The expression for the reststrahl frequency for the point charge model gives the value

$$e_3 = \pm 6.36 \times 10^{-10} \text{esu} ,$$

if the above values of β and γ are used, and McWilliams' (22) value for the reststrahl frequency, $\omega = 5.02 \times 10^{13}$ sec^{-1} is assumed.

With McWilliams' values for the high and low frequency dielectric constants,

$$\epsilon = 13.3$$

$$\epsilon_o = 21.2 ,$$

the reststrahl frequency, and the above values of β and γ, the shell model expressions for these three parameters can be solved for e_1, e_3, and δ, giving

$$e_1 = -24.5 \times 10^{-10} \text{esu}$$

$$e_3 = 6.23 \times 10^{-10} \text{esu or } 2.77 \times 10^{-10} \text{esu}$$

$$\delta = 31.2 \times 10^{4} \text{ d/cm} ,$$

assuming e_1 is negative.

For the calculations which follow, the values of β and γ obtained from the elastic constants and the values for δ, e_1, and e_3 obtained from the reststrahl frequency and dielectric constants with the shell model were used;

$$\beta = 2.26 \times 10^4 \text{ d/cm}$$
$$\gamma = 2.78 \times 10^4 \text{ d/cm}$$
$$\delta = 31.2 \times 10^4 \text{ d/cm}$$
$$e_1 = -24.5 \times 10^{-10} \text{esu}$$
$$e_3 = 6.23 \times 10^{-10} \text{esu} .$$

The higher value of e_3 was chosen because it was consistent with the values obtained from the elastic constants and reststrahl frequency with the point charge model. This does not imply that the magnesium atom actually has such a charge since the introduction of more force constants would certainly change this value.

4. Frequency spectrum

The lattice vibration frequencies for both models were calculated at several points along the [100], [111], and [110] directions in reciprocal space. The shell model was unstable at short wave lengths, yielding imaginary frequencies for some shear modes. Similar effects have been observed by other authors (15) when too simple a model was employed. The results for the point charge model are shown in

Figures 6, 7, and 8. The frequencies for the upper longitudinal optic branches are probably too high, since the Lyddane-Sachs-Teller relation is not satisfied. The frequencies of the longitudinal modes given by the shell model in the [100] direction are shown in Figure 9 for comparison.

A crude approximation to the frequency distribution was obtained by finding the number of modes per unit solid angle in $d\omega$, $q^2\, dq/d\omega$, for each branch in the three directions. The distributions for each branch were weighted by the number of equivalent directions in 4π steradians (6 for the [100] direction, 8 for the [111] direction, and 12 for the [110] direction), added, and normalized. This process is less elegant than the method described by Houston (23), but seems at least as plausible.

The infinities in the resulting distribution were replaced by rectangles of equal area with a frequency width of approximately 10% of the total frequency width of each branch. It has been pointed out (10) that the singularities in a frequency distribution calculated in this manner are certainly spurious, since they are peculiar to these three directions and would be removed in a sum over the entire Brillouin zone. The specific heat is, regardless, quite insensitive to the exact shape of the frequency distribution. To make the calculations easier, the frequency distribution was evaluated as a histogram with a frequency

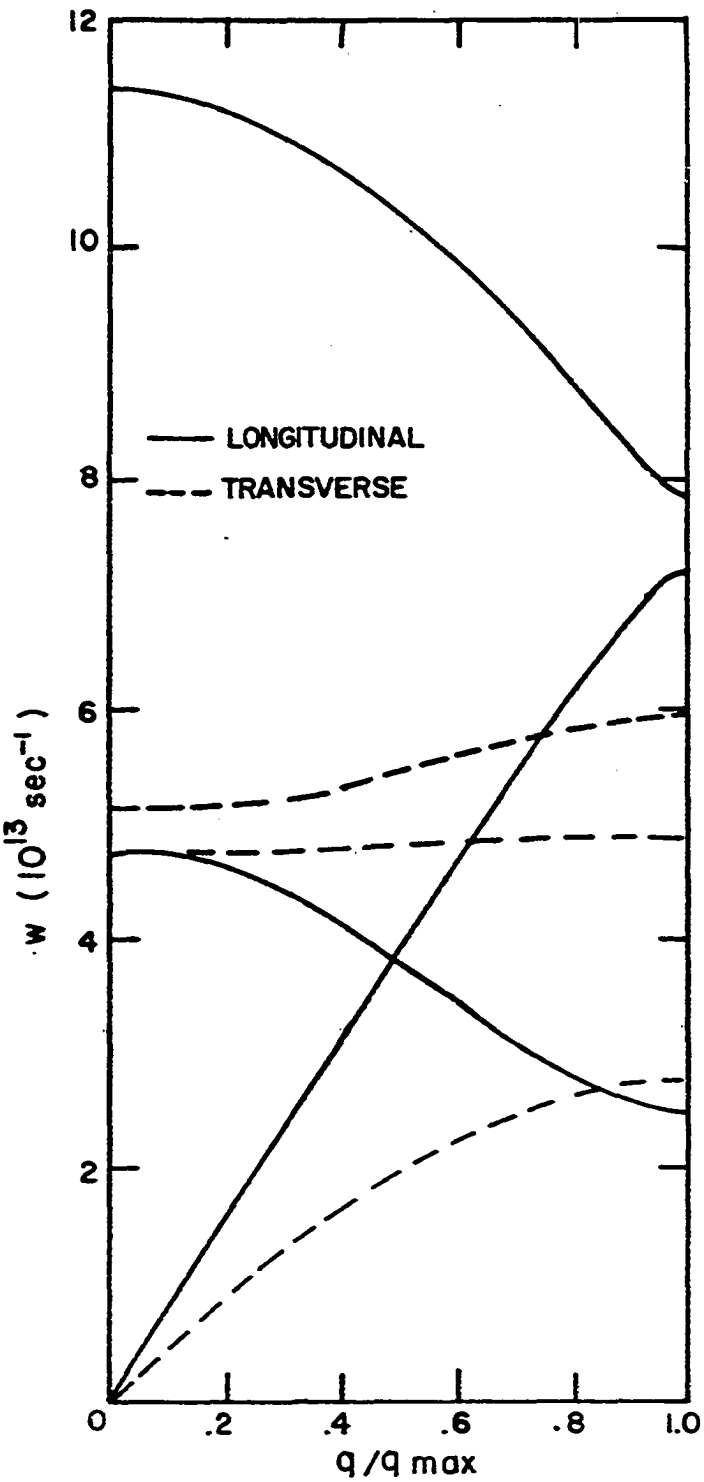

Figure 6. Lattice frequencies versus q, [100] direction

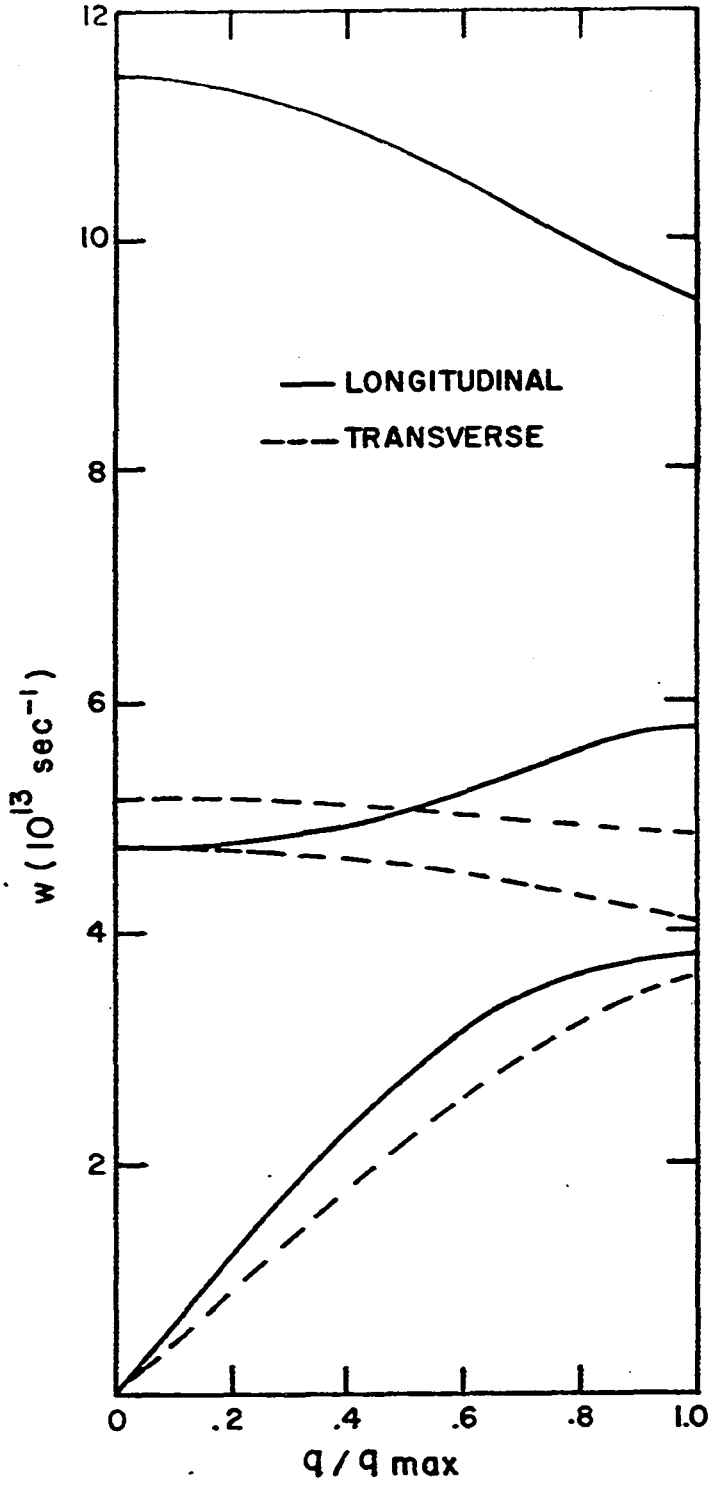

Figure 7. Lattice frequencies versus q, [111] direction

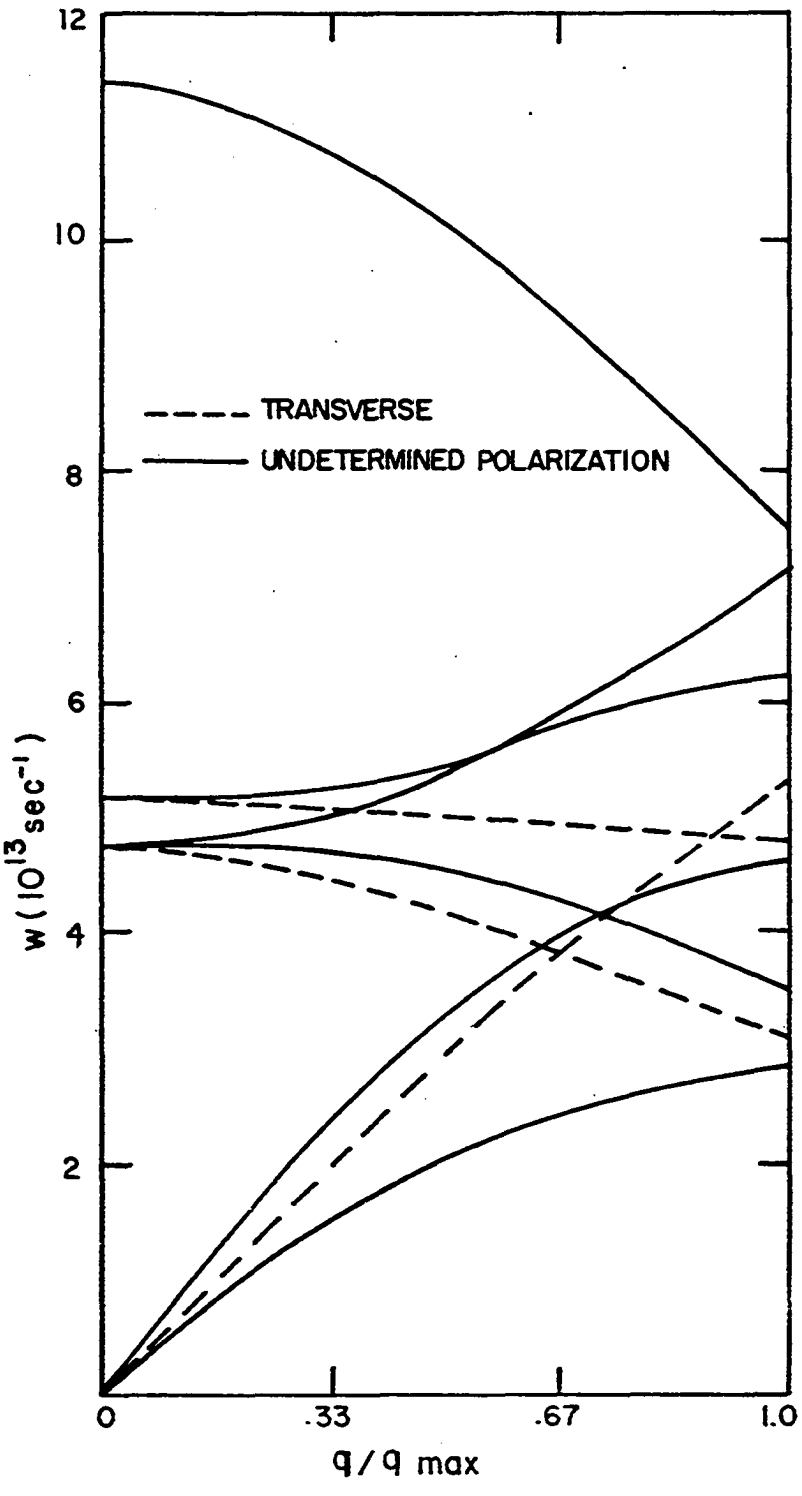

Figure 8. Lattice frequencies versus q, [110] direction

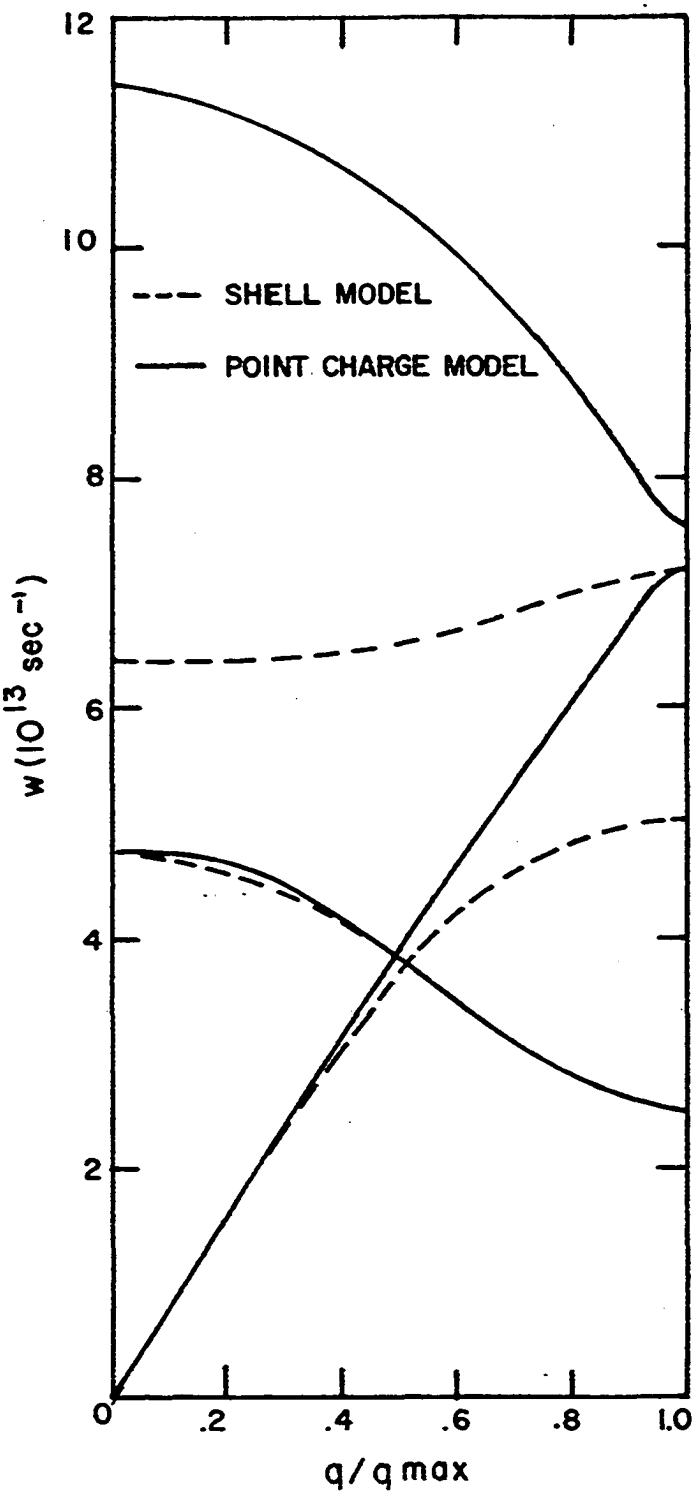

Figure 9. Lattice frequencies versus q, [100] direction

increment, $\Delta\omega$, of 0.2×10^{13} sec^{-1}. This distribution, $n(\omega)\Delta\omega$, is shown in Figure 10.

C. Specific Heat

The energy associated with the lattice vibrations and its temperature derivative, the specific heat at constant volume, C_v, can be readily calculated if the frequency distribution of the vibrations is known. Except at very low temperatures, the specific heat of the lattice vibrations comprises a large fraction of the total specific heat of many materials. A calculation of the lattice specific heat furnishes, therefore, a useful, if not very sensitive check on the accuracy of the frequency distribution.

The quantity which is usually determined experimentally is the specific heat at constant pressure, C_p. The two specific heats, C_p and C_v, are related thermodynamically by (24, p. 265)

$$C_p - C_v = v\beta^2/K \qquad \text{(Eq. 34)}$$

where v is the molar volume, β is the volume expansivity, and K is the compressibility. As the quantity on the right in Equation 34 is often not known for the entire temperature range, an approximate expression, the Nernst-Lindemann relation (24, p. 266), is generally employed to obtain C_v

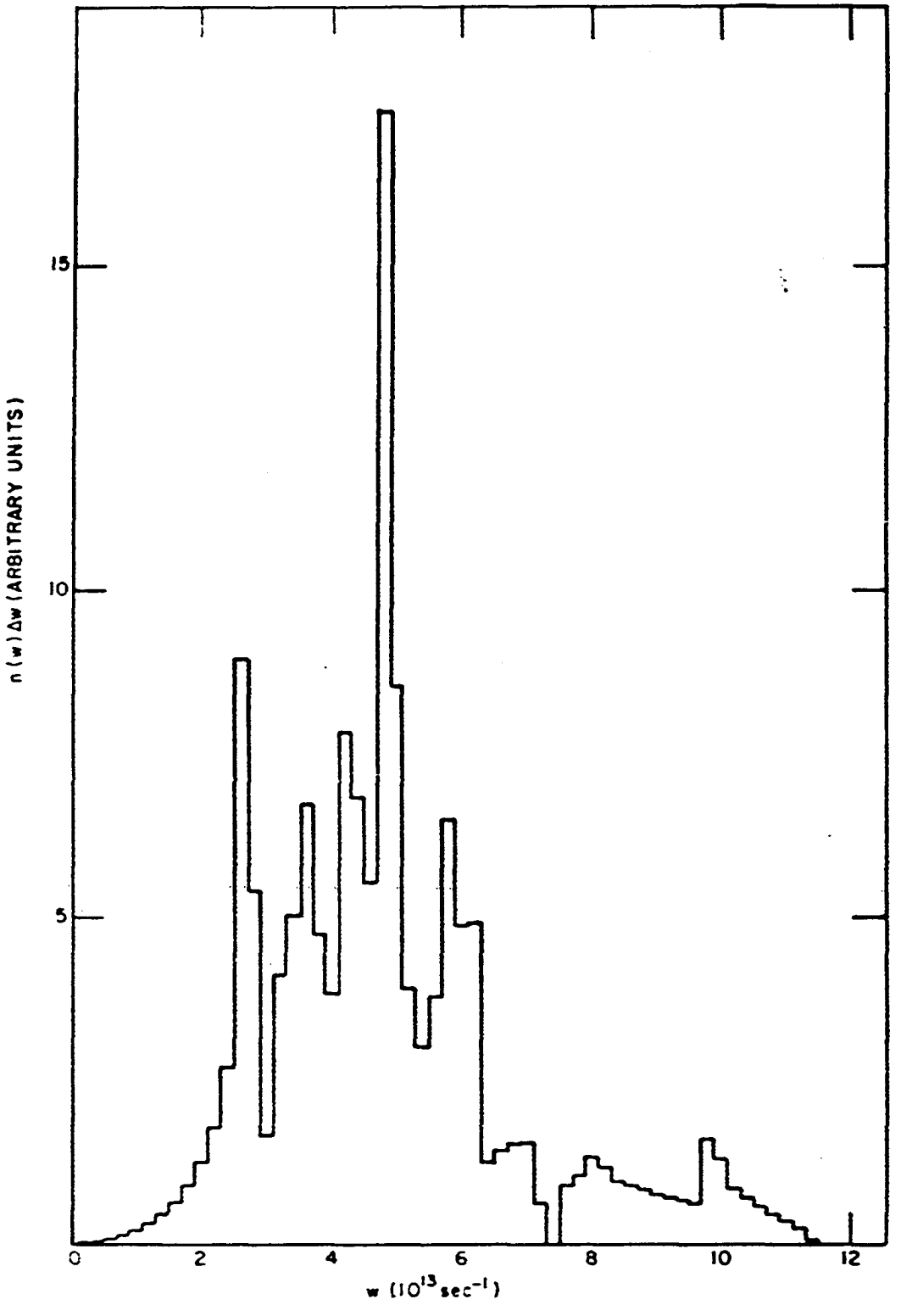

Figure 10. Lattice vibration frequency distribution

from the experimental values of C_p. The Nernst-Lindemann relation can be written

$$C_p - C_v = (v\beta^2/KC_p^2)\, C_p^2\, T = A\, C_p^2\, T\ . \qquad \text{(Eq. 35)}$$

The parameter A is assumed to be independent of temperature. Thus the specific heat at constant volume, C_v, can be obtained from C_p if the value of A can be found at one temperature.

The specific heat of magnesium silicide was calculated at several temperatures from the expression

$$C_v = 3N \frac{\Sigma\, E\, (\frac{\hbar\omega}{kT})\, n(\omega)\Delta\omega}{\Sigma\, n(\omega)\Delta\omega} \qquad \text{(Eq. 36)}$$

where

$$E(x) = k\, x^2\, e^x/(e^x - 1)^2 \qquad \text{(Eq. 37)}$$

is the specific heat of a single oscillator with frequency ω (25, p. 38), N is the number of atoms per unit volume, $\hbar$ is Planck's constant divided by 2π, and k is the Boltzmann constant. Since $n(\omega)\Delta\omega$ was obtained in histogram form, and E(x) is a slowly varying function of the temperature, the summations in Equation 36 were used instead of the customary integrals. This procedure simplified the calculations

considerably, and is certainly consistent with the approximations used to find $n(\omega)\Delta\omega$.

The values obtained from Equation 36 are listed in Table 3, and shown in Figure 11 along with the experimental values of C_p determined by Schimpff (26) and Schübel (27), and values calculated with the Debye model (10). A graph such as Figure 11 is usually not very meaningful, since the Einstein and Debye approximations (10) could no doubt be adjusted to give an equally good fit to the experimental data. It must be remembered though, that all adjustable parameters in this calculation were evaluated from the elastic constants and reststrahl frequency, so the calculated C_v is independent of the experimental C_p.

Table 3. Calculated specific heat and Debye temperature

$T(^{\circ}K)$	C_v(cal/mole $^{\circ}K$)	$\theta_D(^{\circ}K)$
15.85	3.307×10^{-2}	551.6
25.12	1.754×10^{-1}	501.2
39.81	8.977×10^{-1}	459.5
63.10	3.140	457.7
100.0	7.183	473.1
158.5	11.55	491.7
251.2	14.72	506.2
398.1	16.47	514.0

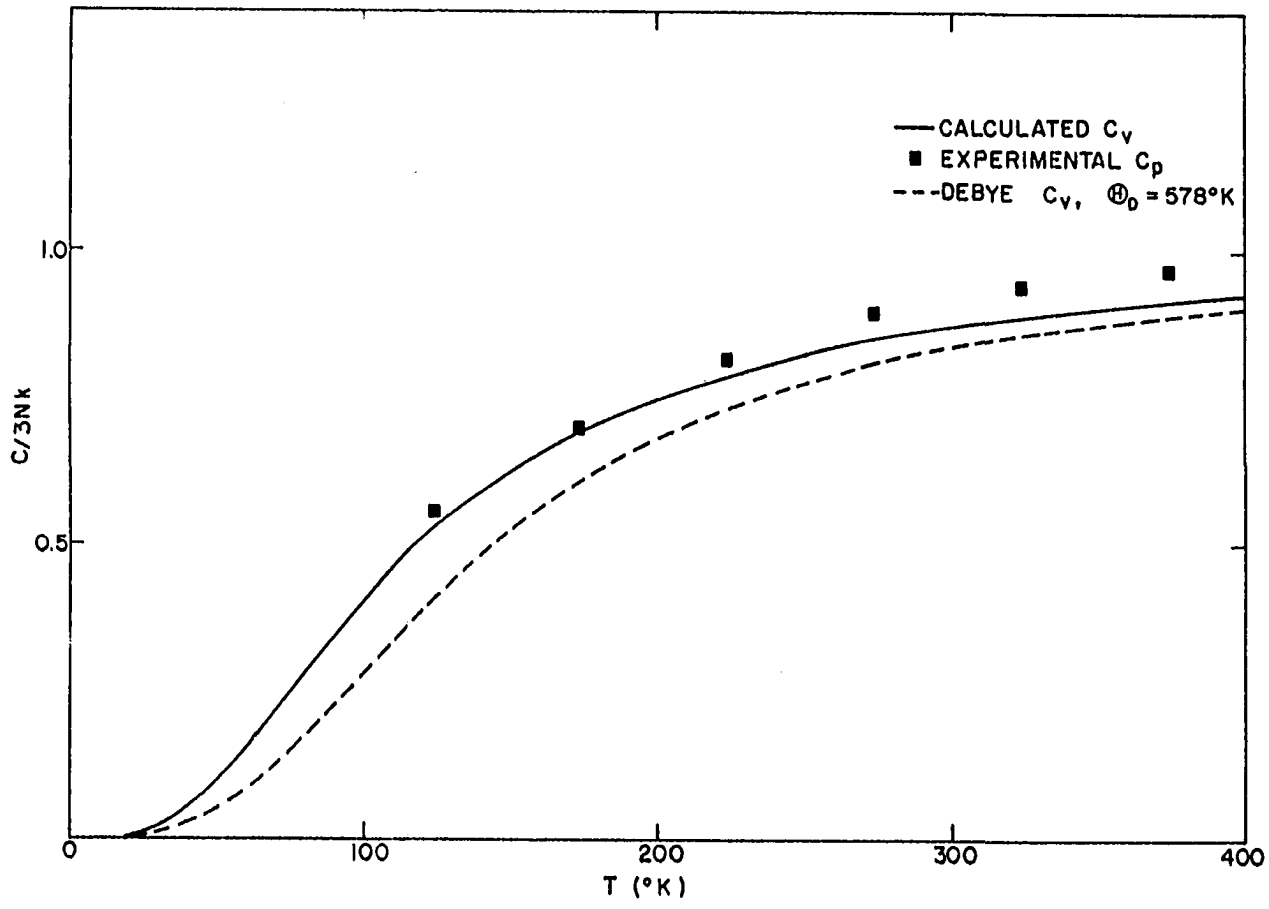

Figure 11. Specific heat of magnesium silicide

The results of the specific heat calculations are displayed in the conventional manner in Figure 12 where an effective Debye temperature is plotted versus temperature. The Debye temperatures were obtained from the table compiled by Beattie (28). The experimental points shown are values determined from the experimental values of C_p and the Nernst-Lindemann relation in a rather devious way. As shown in Table 4, the experimental values of C_v were in some cases greater than 3Nk, 17.88 cal/mole ^{o}K, when the value, 0.273×10^{-5} mole/cal, calculated for A at room temperature was used. When $A = 1.044 \times 10^{-5}$ mole/cal was used, obtained by adjusting the experimental values to the theoretical curve at 323 ^{o}K, the experimental Debye temperatures soared alarmingly at higher temperatures. The values for θ_D were more reasonable at all temperatures when the experimental point at 873 ^{o}K was adjusted to fit the theoretical curve, with $A = 0.749 \times 10^{-5}$ mole/cal, so this value for A was used for the points in Figure 11. Although the values for θ_D at the higher temperatures are quite indefinite, the values at the two lower temperatures are fairly independent of the choice for A, so the agreement of the calculations with these points can be considered a fair test of the model.

At very low temperatures, the Debye temperature can be obtained directly from the elastic constants. In this limit, the specific heat can be expressed (18, p.130)

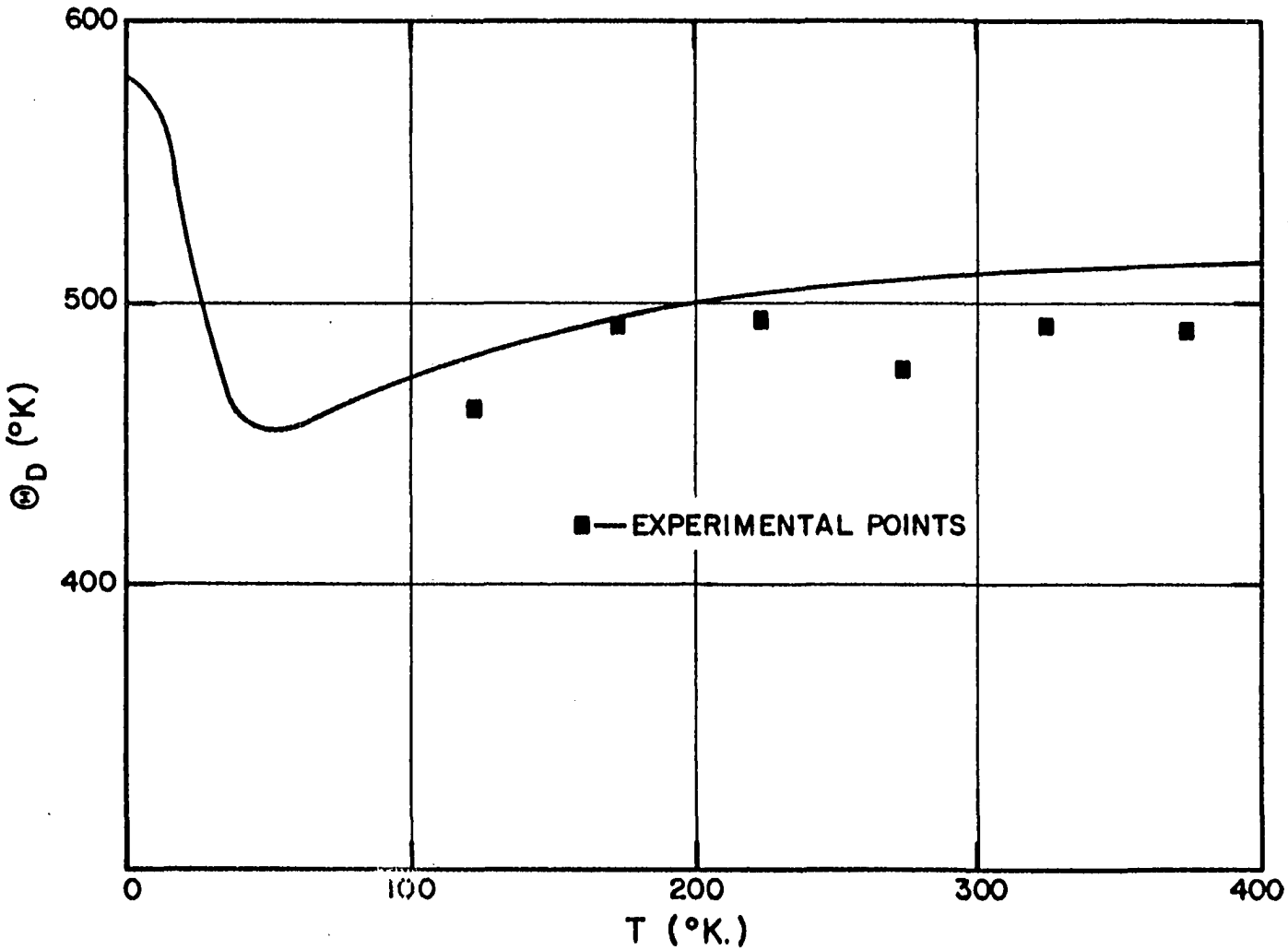

Figure 12. Debye temperature versus temperature

Table 4. Experimental values for C_p, C_v, and θ_D, for different values of the Nernst-Lindemann constant

	T (°K)							
	123	173	223	273	323	373	573	873
C_p (cal/mole °K)	9.89	12.49	14.52	15.95	16.78	17.26	18.83	20.25
A = 0.273×10^{-5} mole/cal								
C_v (cal/mole °K)	9.86	12.42	14.39	15.76	16.53	16.96	18.28	19.27
θ_D (°K)	453.9	486.1	475.0	439.5	407.0	387.9	-	-
A = 0.749×10^{-5} mole/cal								
C_v (cal/mole °K)	9.67	12.29	14.17	15.43	15.97	16.43	17.31	17.57
θ_D (°K)	461.5	493.4	493.3	476.1	491.3	489.7	468.7	520.0
A = 1.044×10^{-5} mole/cal								
C_v (cal/mole °K)	9.76	12.21	14.03	15.22	15.83	16.10	16.71	16.51
θ_D (°K)	457.6	498.1	504.2	498.8	511.0	546.4	671.6	1111

$$C_v/Nk = \frac{12\pi^4}{5} (T/\theta_D)^3 , \qquad \text{(Eq. 38)}$$

where

$$\theta_D = (6\pi^2 N)^{1/3} \hbar\bar{v}/k . \qquad \text{(Eq. 39)}$$

In the above expressions, $\bar{v}$ is an average sound velocity which can be determined from the elastic constants. This is in general a difficult task, but the strong elastic isotropy of magnesium silicide suggests the use of a suitable approximation. Born and von Karman (29) have derived the following relationship for nearly isotropic solids:

$$3/\bar{v}^3 = \rho^{3/2} [2/C_{44}^{3/2} + 1/C_{11}^{3/2} + \frac{3}{5} (C_{12} - C_{11} + 2C_{44})(1/C_{44}^{5/2} - 1/C_{11}^{5/2})] . \qquad \text{(Eq. 40)}$$

Using this expression and the constants,

$$C_{11} = 12.12 \times 10^{11} \text{ d/cm}^2,$$
$$C_{12} = 2.20 \times 10^{11} \text{ d/cm}^2,$$
$$C_{44} = 4.65 \times 10^{11} \text{ d/cm}^2,$$
$$\rho = 2.00 \text{ g/cm}^3,$$

we obtain a value for θ_D of 578 ^{o}K.

An average velocity may also be obtained by the method used to find the frequency distribution;

$$1/\overline{v}^3 = \frac{1}{78}\left[6/v^3_{L100} + 12/v^3_{S100} + 8/v^3_{L111} + 16/v^3_{S111} + 12/v^3_{L110} + 12/v^3_{SI110} + 12/v^3_{SII110}\right], \quad \text{(Eq. 41)}$$

where v_{L100} is the longitudinal velocity in the [100] direction etc. With the constants given above, a value of 578 ^{o}K was again found for θ_D.

The general agreement of these calculations of C_v with experiment is fairly good. Some experimental data at lower temperatures would certainly help to evaluate the model, especially since the difference between C_p and C_v decreases as $C_p^2 T$ as the temperature is lowered. The unusually large difference between C_p and C_v at high temperatures is probably due to experimental errors which become quite significant in this temperature range.

D. Bonding and Ionicity

Several authors have speculated on the chemical bond in the compound, magnesium silicide. The crystal structure is characteristic of many ionic compounds, such as calcium fluoride and barium chloride. However, magnesium plumbide has the same structure and is apparently metallic. Mooser

and Pearson (30) have attributed the semiconducting properties of the similar compound, magnesium stannide, to a covalent bonding scheme in which the two valence electrons of the magnesium atoms are shared equally with the four nearest tin atoms, and the four valence electrons of a tin atom are shared with the eight neighboring magnesium atoms. This viewpoint has been supported by the x-ray diffraction work of Ageev and Guseva (31) on magnesium silicide. They found a large charge density along the lines joining the nearest neighbors, pointing to a considerable amount of covalent bonding. On the basis of his cohesive energy measurements, Caulfield (32) also predicted a predominantly covalent bond. On the other hand, some ionicity must be attributed to the bond to explain the difference between the high and low frequency dielectric constants observed by McWilliams (22).

The results of this investigation favor a mixture of covalent and ionic bonding. The expressions for the elastic constants in terms of the force constants and charges cannot be satisfied with real values of the parameters when the non-central interaction between the magnesium and silicon atoms is replaced by a central interaction between neighboring magnesium atoms. This behavior indicates that directional bonds are important. The relative magnitudes of the three elastic constants of magnesium silicide resemble more those

of the covalent semiconductors, diamond, silicon, and germanium, than those of calcium fluoride, as shown in Table 5.

The charge on the magnesium atoms used in the lattice vibration calculations (~ -1.3 electrons) gives a cohesive energy much larger than the value measured by Caulfield (32). He determined the binding energy of one magnesium atom to be 44.41 kcal/mole. A rough calculation of the coulomb contribution to the cohesive energy by the Ewald technique (18, p. 571) shows that for purely ionic bonding, each magnesium atom accounts for about 0.175 of the cohesive energy per molecule, giving a total cohesive energy of 254 kcal/mole. From this number and the room temperature compressibility, 1.82×10^{-12} cm^2/d, from the elastic constants, an upper limit of ± 0.66 electrons is found for the magnesium charge.

That the charge determined from the elastic constants is larger than this result is not surprising, since only two force constants were assumed. A charge of either -1.3 or -0.58 electrons satisfies the expressions derived for the shell model, but the larger value was chosen for the calculations since it gave good results with the point charge model as well. An estimate of 25% ionic and 75% covalent bonding in magnesium silicide is fairly consistent with the above considerations.

Table 5. Room temperature elastic constants of various materials

Material	$C_{11}(10^{11}$ d/cm$^2)$	$C_{12}(10^{11}$ d/cm$^2)$	$C_{44}(10^{11}$ d/cm$^2)$
Mg_2Si[a]	12.06	2.22	4.64
CaF_2[b]	16.4	5.3	3.370
Diamond[c]	107.6	12.50	57.58
Si[c]	16.57	6.39	7.96
Ge[c]	12.89	4.83	6.71

[a]Present investigation.

[b]See Huffman and Norwood (33).

[c]Tabulated by Huntington (6).

V. SUMMARY

The present investigation has demonstrated the usefulness of resonance techniques for measuring the elastic properties of small specimens of poor crystal quality. While the method is neither as convenient nor as accurate as the pulse-echo technique which works so well with most materials, it can provide useful data for materials with a large acoustic attenuation coefficient.

The lattice vibration frequencies which were calculated are probably inaccurate at the shorter wave lengths, and the longitudinal optic mode frequencies for the higher branch are certainly too high, since the polarization of the atoms was neglected in the point charge model. However, the agreement between the calculated and experimental values for the reststrahl frequency is surprising. When the three parameters determined from the elastic constants from Equations 18 are used, a value for the reststrahl frequency of $\omega = 5.83 \times 10^{13}$ sec^{-1} is obtained, whereas McWilliams (22) experimentally obtained the value $\omega = 5.03 \times 10^{13}$ sec^{-1}.

An evaluation of the specific heat calculations is hindered by the lack of low temperature experimental data. The values obtained for the point charge model seem to agree fairly well with the experimental points which are available.

It is felt that the results of the present investigation furnish a reasonable description of the phonons in magnesium silicide at thermal equilibrium. If future investigations can determine the constant energy surfaces and effective masses of the electrons in this material, it is possible that many of the transport properties can be explained.

VI. LITERATURE CITED

1. Heller, M. W. and G. C. Danielson. Seebeck effect in Mg_2Si single crystals. Journal of Physics and Chemistry of Solids 23: 601. 1962.

2. Morris, R. G., R. D. Redin, and G. C. Danielson. Semiconducting properties of Mg_2Si single crystals. Physical Review 109: 1909. 1958.

3. Winkler, U. Die electrischen Eigenschaften der intermetallischen Verbindungen Mg_2Si, Mg_2Ge, Mg_2Sn und Mg_2Pb. Helvetica Physica Acta 28: 633. 1955.

4. Koenig, P., D. W. Lynch, and G. C. Danielson. Infrared absorption in magnesium silicide and magnesium germanide. Journal of Physics and Chemistry of Solids 20: 122. 1961.

5. DeLaunay, J. The theory of specific heats and lattice vibrations. Solid State Physics 2: 219. 1956.

6. Huntington, H. B. The elastic constants of crystals. Solid State Physics 7: 213. 1958.

7. Bolef, D. I. and M. Menes. Measurement of elastic constants of RbBr, RbI, CsBr, and CsI by an ultrasonic cw resonance technique. Journal of Applied Physics 31: 1010. 1960.

8. Bolef, D. I. Elastic constants of single crystals of the bcc transition elements V, Nb, and Ta. Journal of Applied Physics 32: 100. 1961.

9. Williams, J. and J. Lamb. On the measurement of ultrasonic velocity in solids. Journal of the Acoustical Society of America 30: 308. 1958.

10. Blackman, M. The specific heat of solids. In Flügge, S., ed. Handbuch der Physik. Vol. 7. pp. 325-382. Berlin, Springer-Verlag. 1955.

11. Blackman, M. Contributions to the theory of the specific heat of crystals. II. On the vibrational spectrum of cubical lattices and its application to the specific heat of crystals. Royal Society of London Proceedings, Series A, 148: 384. 1935.

12. Born, M. and K. Huang. Dynamical theory of crystal lattices. Oxford, Clarendon Press. 1954.

13. Kellermann, E. W. Theory of the vibrations of the sodium chloride lattice. Philosophical transactions of the Royal Society of London, Series A, 238: 513. 1940.

14. Cochran, W. Theory of the lattice vibrations of germanium. Royal Society of London Proceedings, Series A, 253: 260. 1959.

15. Woods, A. D. B., W. Cochran, and B. N. Brockhouse. Lattice dynamics of alkali halide crystals. Physical Review 119: 980. 1960.

16. Ganesan, S. and R. Srinivasan. Lattice dynamics of calcium fluoride. Part I. Lyddane, Sachs, Teller formula, diffuse x-ray scattering, and specific heat. Canadian Journal of Physics 40: 74. 1962.

17. Srinivasan, R. Elastic constants of calcium fluoride. Physical Society of London Proceedings 72: 566. 1958.

18. Kittel, C. Introduction to solid state physics. 2nd ed. New York, New York, John Wiley and Sons, Inc. 1956.

19. Kaplan, H. and J. Sullivan. Lattice vibrations of zincblende structure crystals with application to ZnS. U. S. Atomic Energy Commission report AFOSR-2300. [Air Force Office of Scientific Research, Washington, D. C.] 1961.

20. Rajagopal, A. K. Closed shell ion-ion interactions in calcium fluoride. Journal of Physics and Chemistry of Solids 23: 317. 1962.

21. Lyddane, R. H., R. G. Sachs, and E. Teller. On the polar vibrations of alkali halides. Physical Review 59: 673. 1941.

22. McWilliams, D. A. Infrared indices of refraction and reflectivities of Mg_2Si, Mg_2Ge, and Mg_2Sn. Unpublished Ph.D. thesis. Ames, Iowa, Library, Iowa State University of Science and Technology. 1962.

23. Houston, W. V. Normal vibrations of a crystal lattice. Reviews of Modern Physics 20: 161. 1948.

24. Zemansky, M. W. Heat and thermodynamics. 3rd ed. New York, New York, McGraw-Hill Book Co., Inc. 1951.

25. Dekker, A. J. Solid state physics. Englewood Cliffs, New Jersey, Prentice-Hall, Inc. 1957.

26. Schimpff, H. Über die Wärmekapazität von Metallen und Metallverbindungen. Zeitschrift für physikalische Chemie 71: 257. 1910.

27. Schübel, P. Über die Wärmekapazität von Metallen und Metallverbindungen zwischen 18-600°. Zeitschrift für anarganische Chemie 87: 81. 1914.

28. Beattie, J. A. Six place tables of the Debye energy and specific heat functions. Journal of Mathematics and Physics 6: 1. 1926.

29. Born, M. and T. von Karman. Zur Theorie der spezifischen Wärme. Physikalische Zeitschrift 14: 15. 1913.

30. Mooser, E. and W. B. Pearson. Chemical bond in semiconductors. Journal of Electronics 1: 629. 1956.

31. Ageev, N. V. and L. N. Guseva. Experimental study of the electron density in crystals. Communication V. Electron density of Mg_2Si. Academy of Sciences U. S. S. R. Division of Chemical Sciences Bulletin 1: 31. 1952.

32. Caulfield, H. J. Cohesion in the intermetallic series Mg_2Si, Mg_2Ge, Mg_2Sn, and Mg_2Pb. Unpublished Ph.D. thesis. Ames, Iowa, Library, Iowa State University of Science and Technology. 1962.

33. Huffman, D. R. and M. H. Norwood. Specific heat and elastic constants of calcium fluoride at low temperatures. Physical Review 117: 709. 1960.

VII. ACKNOWLEDGMENTS

I would like to thank my major professor, Dr. G. C. Danielson, who suggested the problem and offered much encouragement throughout the investigation; also, Dr. Marvin Heller and Mr. William Smith who furnished the crystals for the specimens. Dr. R. H. Good and Dr. J. M. Keller assisted with the theoretical aspects of the lattice vibration calculations; Mr. John Kennealy wrote the computer programs and helped to find the frequency distribution. Mrs. Evelyn Blair performed many of the miscellaneous calculations.

VIII. APPENDIX A: SOUND VELOCITY DATA

The sound velocities in the [110] and [111] directions which were used in the calculations are given in Tables 6 through 10.

Table 6. Sound velocity, [110] direction, longitudinal wave

T(°K)	$v_L(10^5$ cm/sec)	T(°K)	$v_L(10^5$ cm/sec)
81	7.793	152	7.769
		164	7.769
81	7.802	174	7.726
98	7.805		
113	7.790	152	7.742
127	7.777	164	7.730
140	7.762	174	7.736
152	7.750	185	7.713
164	7.765		
174	7.707	164	7.790
185	7.750	174	7.802
195	7.757	185	7.784
205	7.713	195	7.778
214	7.693	205	7.775
223	7.663	214	7.758
232	7.704	223	7.773
81	7.814	246	7.715
		254	7.701
81	7.794	263	7.695
98	7.838	266	7.694
113	7.769	278	7.694
127	7.772	286	7.686
140	7.771	294	7.689
		300	7.685

Table 7. Sound velocity, [110] direction, shear wave I

T(°K)	$v_{SI}(10^5$ cm/sec)	T(°K)	$v_{SI}(10^5$ cm/sec)
81	4.896	195	4.858
98	4.891	205	4.858
113	4.895	214	4.845
127	4.884	223	4.847
140	4.880		
152	4.865	241	4.843
164	4.880	252	4.834
		263	4.828
140	4.876	273	4.827
152	4.871	284	4.821
164	4.866	294	4.813
174	4.867	299	4.815
185	4.861	303	4.809

Table 8. Sound velocity, [110] direction, shear wave II

T(°K)	$v_{SII}(10^5$ cm/sec)	T(°K)	$v_{SII}(10^5$ cm/sec)
81	5.025	195	4.994
98	5.022	205	4.997
113	5.020	214	4.994
127	5.014	223	4.982
140	5.011		
152	5.005	241	4.982
		252	4.981
140	5.011	263	4.974
152	5.006	273	4.969
164	5.010	284	4.967
174	5.001	294	4.961
185	5.003	299	4.960

Table 9. Sound velocity, [111] direction, longitudinal wave

T(°K)	$v_L(10^5$ cm/sec)	T(°K)	$v_L(10^5$ cm/sec)
81	7.778	174	7.749
113	7.770	185	7.739
127	7.775	195	7.735
140	7.787	205	7.741
152	7.752	214	7.732
164	7.738	223	7.702
174	7.723	232	7.674
185	7.709	241	7.684
195	7.705	252	7.655
205	7.746		
214	7.752	263	7.656
223	7.697	273	7.652
		284	7.643
152	7.772	294	7.659
164	7.753	300	7.645

Table 10. Sound velocity, [111] direction, shear wave

T(°K)	$v_S(10^5$ cm/sec)	T(°K)	$v_S(10^5$ cm/sec)
81	4.992	205	4.918
98	4.995	214	4.921
113	4.989	223	4.917
127	4.974	232	4.924
140	4.971		
152	4.971	252	4.948
		263	4.942
164	4.942	273	4.937
174	4.925	284	4.935
185	4.940	294	4.934
195	4.923	300	4.936

IX. APPENDIX B: ADIABATIC ELASTIC CONSTANTS

The averages of the elastic constants calculated in the two ways described in Section IV-A are given in Table 11.

Table 11. Adiabatic elastic constants

T(°K)	$C_{11}(10^{11}$ d/cm$^2)$	$C_{12}(10^{11}$ d/cm$^2)$	$C_{44}(10^{11}$ d/cm$^2)$
81	12.35	2.29	4.761
98	12.33	2.31	4.753
113	12.30	2.28	4.761
127	12.31	2.32	4.742
140	12.33	2.34	4.733
152	12.30	2.30	4.725
164	12.29	2.30	4.716
174	12.22	2.26	4.716
185	12.25	2.28	4.707
195	12.26	2.32	4.701
205	12.27	2.32	4.703
214	12.27	2.32	4.681
223	12.16	2.26	4.685
241	12.14	2.24	4.679
252	12.10	2.20	4.664
263	12.10	2.22	4.655
273	12.09	2.22	4.655
284	12.08	2.21	4.646
294	12.11	2.27	4.631
300	12.08	2.24	4.637

X. APPENDIX C: COULOMB COUPLING COEFFICIENTS

The values for the coulomb coupling coefficients used in the lattice vibration calculations are given below. The coefficients $[^{23}_{\alpha\beta}]$ are from Kellermann (13); the remainder are from Kaplan and Sullivan (19).

In the [100] direction, the coupling coefficients have the form:

$$[^{kk}_{\alpha\beta}]\ v/e_k^2 = \begin{pmatrix} 2A & 0 & 0 \\ 0 & -A & 0 \\ 0 & 0 & -A \end{pmatrix},$$

$$[^{12}_{\alpha\beta}]\ v/e_1e_2 = [^{13}_{\alpha\beta}]^*\ v/e_1e_2 = \begin{pmatrix} 2B & 0 & 0 \\ 0 & -B & iC \\ 0 & iC & -B \end{pmatrix},$$

$$[^{23}_{\alpha\beta}]\ v/e_2^2 = \begin{pmatrix} 2D & 0 & 0 \\ 0 & -D & 0 \\ 0 & 0 & -D \end{pmatrix}.$$

Values of the parameters are given in Table 12.

Table 12. [100] parameters for coulomb coupling coefficients

q/q_{max}	A	B	C	D
0	4.189	4.189	0	4.189
.2	4.006	3.979	-3.123	4.491
.4	3.517	3.374	-6.022	5.313
.6	2.893	2.444	-8.424	6.344
.8	3.370	1.281	-10.046	7.193
1.0	2.166	0	-10.624	7.520

In the [111] direction, the coupling coefficients are:

$$[^{kk}_{\alpha\beta}]\ v/e_k^2 = \begin{pmatrix} 0 & A & A \\ A & 0 & A \\ A & A & 0 \end{pmatrix},$$

$$[^{12}_{\alpha\beta}]\ v/e_1e_2 = \begin{pmatrix} 0 & B-iC & B-iC \\ B-iC & 0 & B-iC \\ B-iC & B-iC & 0 \end{pmatrix},$$

$$[^{23}_{\alpha\beta}]\ v/e_2^2 = \begin{pmatrix} 0 & D & D \\ D & 0 & D \\ D & D & 0 \end{pmatrix}.$$

Values for the [111] parameters are given in Table 13.

Table 13. [111] parameters for coulomb coupling coefficients

q/q_{max}	A	B	C	D
0	4.189	4.189	0	4.189
.2	4.131	4.266	-1.547	3.993
.4	3.986	4.471	-2.920	3.421
.6	3.812	4.706	-4.011	2.511
.8	3.668	4.928	-4.657	1.330
1.0	3.615	4.948	-4.948	0

In the [110] direction, the coupling coefficients have the form:

$$[^{kk}_{\alpha\beta}]\ v/e_k^2 = \begin{pmatrix} A & B & 0 \\ B & A & 0 \\ 0 & 0 & -2A \end{pmatrix},$$

$$[^{12}_{\alpha\beta}]\ v/e_1e_2 = \begin{pmatrix} C & D & -iE \\ D & C & -iE \\ -iE & -iE & -2C \end{pmatrix},$$

$$[^{23}_{\alpha\beta}]\ v/e_2^2 = \begin{pmatrix} F & G & 0 \\ G & F & 0 \\ 0 & 0 & -2F \end{pmatrix}.$$

Values for the [110] parameters are given in Table 14. The

values for F and G were interpolated from Kellermann's table. The sign of E at $q = q_{max}$ was changed, the value with the opposite sign giving some negative eigenvalues.

Table 14. [110] parameters for coulomb coupling coefficients

q/q_{max}	A	B	C	D	E	F	G
0	2.095	6.283	2.095	6.283	0	2.095	6.283
.33	1.780	5.874	1.770	6.769	-3.668	2.595	5.100
.67	0.669	4.262	1.018	8.117	-5.694	4.205	2.715
1.0	-1.132	1.546	0.173	9.683	-4.524	5.830	0.130

XI. APPENDIX D: NONCOULOMB COUPLING COEFFICIENTS

Since we are concerned only with nearest-neighbor interactions in the present investigation, many of the indices can be removed from Born's notation. Let $\vec{r}''$ be the vector from (ℓk) to $(\ell''k'')$, let $\vec{x}''$ be the vector between their lattice sites, and let

$$\vec{u}'' = \vec{r}'' - \vec{x}'' \ .$$

The potential energy of (ℓk) can be written,

$$\varphi = \Sigma \varphi'' \qquad \text{(Eq. 42)}$$

where the sum is over the nearest neighbors, and φ'' is the interaction energy between (ℓk) and $(\ell''k'')$. For central interactions, φ'' is assumed to have the form:

$$\varphi_C'' = (\tau/2)(|\vec{r}''| - |\vec{x}''|)^2 \ , \qquad \text{(Eq. 43)}$$

where τ is a force constant determining the strength of the interaction. For noncentral interactions, φ'' is assumed to have the form:

$$\varphi_N'' = (\tau'/2) \left| \frac{-(\vec{u}'' \wedge \vec{x}'') \wedge \vec{x}''}{x''^2} \right|^2 \qquad \text{(Eq. 44)}$$

These expressions were essentially obtained by integrating

the expressions given by DeLaunay (5) for the central and noncentral forces between two elements. When Equations 42, 43, and 44 are substituted into Equation 15, the following expressions for the coupling coefficients are obtained:

$$N_{\alpha\beta}^{[kk']}{}_C = - \sum_{\ell'} \tau \frac{x'_\alpha x'_\beta}{x'^2} e^{i\vec{q}\cdot\vec{x}'} + \delta_{kk'} \sum_{\ell''k''} \tau \frac{x''_\alpha x''_\beta}{x''^2} , \qquad \text{(Eq. 45)}$$

$$N_{\alpha\beta}^{[kk']}{}_N = \sum_{\ell'} \tau' \left(\frac{x'_\alpha x'_\beta}{x'^2} - \delta_{\alpha\beta}\right) e^{i\vec{q}\cdot\vec{x}'} - \delta_{kk'} \sum_{\ell''k''} \tau' \left(\frac{x''_\alpha x''_\beta}{x''^2} - \delta_{\alpha\beta}\right) . \qquad \text{(Eq. 46)}$$

In the above expressions, the first summation is only over those neighbors with the basis k'. The second summation is over all nearest neighbors.

To include all nearest neighbors of the elements in cell 0, six neighboring cells must be considered. The elements and their relative positions are given in Table 15. To simplify the algebra, the force constants

$$\beta = (\tau + 2\tau')/3 ,$$

$$\gamma = (\tau - \tau')/3 ,$$

were used. When the sums are carried out, we obtain Equations 17.

Table 15. Nearest neighbors and their relative positions

ℓ	k	ℓ'	k'	$x_1'(2/4)$	$x_2'(a/4)$	$x_3'(a/4)$
0	1	0	2	-1	-1	-1
0	1	0	3	1	1	1
0	1	1	2	1	-1	1
0	1	2	3	-1	1	-1
0	1	3	2	1	1	-1
0	1	4	3	-1	-1	1
0	1	5	2	-1	1	1
0	1	6	3	1	-1	-1
0	2	0	1	1	1	1
0	2	2	1	-1	1	-1
0	2	4	1	-1	-1	1
0	2	6	1	1	-1	-1
0	3	0	1	-1	-1	-1
0	3	1	1	1	-1	1
0	3	3	1	1	1	-1
0	3	5	1	-1	1	1

XII. APPENDIX E: EVALUATION OF THE ELASTIC CONSTANTS

Born and Huang (12) have developed an expansion technique which yields the elastic constants as functions of the coupling coefficients and their derivatives at q = 0. This method has been applied to the fluorite structure by Srinivasan (17) and Rajagopal (20). The expressions, for the sign conventions of the present investigation, are:

$$
\begin{aligned}
C_{11} &= [11,11] \ , \\
C_{12} &= [11,22] \ , \\
C_{44}^{*} &= [12,12] \ , \\
C_{44} &= C_{44}^{*} - 2\,[{}^{2}_{123}]^{2}/(D + 2D') \ ,
\end{aligned}
\qquad \text{(Eq. 47)}
$$

where

$$
\sum_{\alpha\beta} S_{\alpha}S_{\beta}[1\alpha,2\beta] = (2/a^{3})(\partial^{2}/\partial q^{2} \sum_{kk'} [{}^{kk'}_{12}])_{o} \ ,
$$

$$
D = (-4/a^{3})\,[{}^{12}_{11}]_{o} \ ,
$$

$$
D' = (-4/a^{3})\,[{}^{23}_{11}]_{o} \ ,
$$

$$
i \sum_{\alpha} [{}^{k}_{12\alpha}]\, S_{\alpha} = (4/a^{3})(\partial/\partial q \sum_{k'} [{}^{kk'}_{12}])_{o} \ ,
$$

$$
\vec{q} = q\,\vec{S} \ ,
$$

where $\vec{S}$ is a unit vector in the direction of propagation.

The coulomb portions of the elastic constants have been evaluated numerically by Srinivasan (17) and given in final form by Rajagopal (20). The noncoulomb parts can be obtained from the coupling coefficients derived in the last section and Equations 47. We get:

$$
\begin{aligned}
{}^{N}C_{11} &= (2/a)\beta \ , \\
{}^{N}C_{12} &= (2/a)(2\gamma-\beta) \ , \\
{}^{N}C^{*}_{44} &= (2/a)\beta \ , \\
{}^{N}[^{2}_{123}] &= (-4/a^{2})\gamma \ , \\
{}^{N}D &= (4/a^{3})(-4\beta) \ , \\
{}^{N}D' &= 0 \ .
\end{aligned}
\qquad \text{(Eq. 48)}
$$

When the coulomb terms of Rajagopal (20) are added, the results for the elastic constants are:

$$
\begin{aligned}
aC_{11} &= 3.276 \times 8e^{2}/a^{3} + 2\beta \ , \\
aC_{12} &= -5.395 \times 8e^{2}/a^{3} + 4\gamma - 2\beta \ , \\
aC_{44} &= -1.527 \times 8e^{2}/a^{3} + 2\beta - (2/\beta)(2.519 \times 8e^{2}/a^{3} - \gamma)^{2} \ .
\end{aligned}
\qquad \text{(Eq. 18)}
$$

XIII. APPENDIX F: HIGH AND LOW FREQUENCY DIELECTRIC CONSTANTS

To evaluate the dielectric constants from the shell model, we must calculate the dipole moment per unit volume produced by an external electric field. Since the silicon atoms are centers of symmetry, the polarization will be independent of field direction, so we can choose the x direction for convenience. In the manner of Woods *et al.* (15), we can write,

$$m_k \ddot{u}_l(\ell k) = \sum_{\beta \ell' k'} (\partial^2 N\varphi/\partial u_l \partial u_\beta)_o \, u_\beta(\ell' k') + e_k E_o e^{i\omega_o t}, \qquad \text{(Eq. 49)}$$

where $E_o e^{i\omega_o t}$ is the effective field seen by the element (ℓk). Since we are concerned only with vibrations with $q = 0$, we can substitute in Equation 49.

$$u_l(\ell k) = A_l^k e^{i\omega_o t},$$

obtaining four equations for the four A_l^k:

$$
\begin{aligned}
&(\delta - m_1\omega_o^2)\, A_1^1 - \delta A_1^2 = e_1 E_o \,, \\
&-\delta A_1^1 + (8\beta + \delta)\, A_1^2 - 4\beta A_1^3 - 4\beta A_1^4 = e_2 E_o \,, \\
&-4\beta A_1^2 + (4\beta - m_3\omega_o^2)\, A_1^3 = e_3 E_o \,, \\
&-4\beta A_1^2 + (4\beta - m_3\omega_o^2)\, A_1^4 = e_3 E_o \,.
\end{aligned}
\qquad \text{(Eq. 50)}
$$

The equations are not independent, however, since the sum of all four vanishes identically for charge neutrality. It is easily seen that

$$A_1^3 = A_1^4 \,. \qquad \text{(Eq. 51)}$$

The polarization is given by,

$$P = (1/v)(e_1 A_1^1 + e_2 A_1^2 + e_3 A_1^3 + e_3 A_1^4) \,,$$

where v is the volume of the primitive cell. If we require charge neutrality,

$$e_1 + e_2 + 2e_3 = 0 \,,$$

we can write,

$$P = (1/v)[e_1(A_1^1 - A_1^3) + e_2(A_1^2 - A_1^3)] \,. \qquad \text{(Eq. 52)}$$

For $\omega_o = 0$, Equations 50 can be written,

$$(8\beta + \delta)(A_1^2 - A_1^3) - \delta(A_1^1 - A_1^3) = e_2 E_o \ ,$$

$$-4\beta(A_1^2 - A_1^3) = e_3 E_o \ , \qquad \text{(Eq. 53)}$$

giving,

$$P/E_o = (1/v)[-e_1 e_3(8\beta + \delta) - 4\beta e_1 e_2 - \delta e_2 e_3]/4\beta\delta \ ,$$

and with some manipulation,

$$P/E_o = (1/v)\left\{ e_2^2/(8\beta + \delta) + 2[e_3 + 4\beta e_2/(8\beta + \delta)]^2(8\beta + \delta)/4\beta\delta \right\} . \qquad \text{(Eq. 29)}$$

For $\omega_o = \infty$, it is apparent that,

$$A_1^1 = A_1^3 = 0 \ ,$$

$$A_1^2 = e_2 E_o/(8\beta + \delta) \ ,$$

so

$$P/E_o = (1/v)\ e_2^2/(8\beta + \delta) \ . \qquad \text{(Eq. 30)}$$

This quantity represents the polarizability per unit volume of the massless shell of the silicon atom, so it is

reasonable to call the remainder of Equation 29 the ionic polarizability per unit volume.